Investigation of Electromagnetic Interference of PWM Motor Drives in Automotive Electrical Systems

by

Feng Zhang

Submitted to the Department of Electrical Engineering and Computer Science
in partial fulfillment of the requirements for the degree of

Master of Science

at the

MASSACHUSETTS INSTITUTE OF TECHNOLOGY

May 1999

June 1999

Author .....
Department of Electrical Engineering and Computer Science
May 18, 1999

Certified by .....
John G. Kassakian
Professor of Electrical Engineering and Computer Science
Thesis Supervisor

Certified by .....
Stephan H. Guttowski
Visiting Scientist
Thesis Supervisor

Accepted by .....
Arthur C. Smith
Chairman, Department Committee on Graduate Students

Investigation of Electromagnetic Interference of PWM Motor Drives in Automotive Electrical Systems

by

Feng Zhang

Submitted to the Department of Electrical Engineering and Computer Science
on May 18, 1999, in partial fulfillment of the
requirements for the degree of
Master of Science

Abstract

In this thesis, the EMI behavior of PWM dc motor drives for automotive applications is investigated. A theoretical model for the spectrum of the line current for a typical PWM motor drive is first developed. A PWM motor drive is then designed and constructed and an experimental setup is developed for measuring the EMI level generated by this PWM motor drive. Experimental measurements are recorded and analyzed for this PWM drive circuit under different loads and electrical parameters. Finally, an EMI filter is designed, constructed and tested for this PWM drive.

Thesis Supervisor: John G. Kassakian
Title: Professor of Electrical Engineering and Computer Science

Thesis Supervisor: Stephan H. Guttowski
Title: Visiting Scientist

Contents

1 Introduction **1**

1.1 Why PWM Control? 1

1.2 Research Objectives 1

1.3 Thesis Organization 2

2 Theoretical Background **4**

2.1 EMI Calculation for a PWM dc Motor Drive 5

2.2 EMI Classification 9

2.2.1 Classification by Frequency Content 9

2.2.2 Classification by Transmission Mode 10

2.3 Investigation and Reduction of Conducted EMI 11

2.4 Definition of Insertion Loss 11

2.5 Standard SAE J1113/41 13

3 Experimental Setup **16**

3.1 Test Bench Layout 16

3.2 Loads 17

3.3 PWM Motor Drive Circuit 17

3.4 Rectangular Wave Generator and Power Supplies 19

3.5 LISN 21

4 EMI Measurement without EMI Filter **24**

4.1 EMI Measurement under Different Load Conditions 25

4.1.1 Time Domain Measurement for the 42 V Motor 25

4.1.2 Time Domain Measurement for the 14 V Motor 29

4.1.3 Frequency Domain Measurement for Both Motors 31
4.2 EMI Measurement with Different Gate Resistance 33
4.3 Insertion Loss Requirement for the EMI Filter 36

5 EMI Filter Design **40**
5.1 EMI Filter Topologies 41
5.1.1 The π Filter 41
5.1.2 T Filter 42
5.1.3 L Filter 43
5.2 EMI Filter Requirements 44
5.3 Capacitor Value for the L Filter 44
5.4 Damping and Inductor Value for the L Filter 46
5.5 Filter Component Selection and Layout 48

6 EMI Measurement with EMI Filter **51**
6.1 EMI Measurement before Modification 51
6.2 EMI Measurement after Modification 52
6.3 Further Improvement 54

7 Conclusion **57**

A Insertion Loss Calculation **59**

B Matlab Code **62**

List of Figures

2-1 EMC/EMI overview. 4
2-2 Line current waveform for a typical PWM drive with a resistive load. 6
2-3 Calculated spectrum for a typical PWM drive input current. 7
2-4 Differential mode and common mode current. 10
2-5 Insertion loss definition. 12

3-1 Test bench layout for EMI measurement. 17
3-2 PWM dc motor drive circuit diagram. 18
3-3 Rectangular wave generator. 20
3-4 Line Impedance Stabilization Network (LISN). 21
3-5 LISN equivalent circuit. 22
3-6 Calculated load side impedance of the LISN. 22
3-7 Measured and calculated insertion loss of the LISN. 23

4-1 Control signal and line current for 50% duty ratio. 26
4-2 Control signal and line current for 30% duty ratio. 26
4-3 Control signal and line current for 20% duty ratio. 27
4-4 Voltage across the EMI measurement output on the LISN. 27
4-5 Voltage across the load side of the LISN. 28
4-6 Voltage across the power supply side of the LISN. 28
4-7 Control signal and line current for 50% duty ratio. 29
4-8 Control signal and line current for 30% duty ratio. 30
4-9 Control signal and line current for 20% duty ratio. 30
4-10 The ac circuit model for the measurement circuit. 31
4-11 Measured and calculated spectrum for the noise from 150 kHz to 30 MHz. . 32

4-12 Spectrum measured from 150 kHz to 30 MHz. 34
4-13 Spectrum measured from 30 MHz to 108 MHz. 35
4-14 Spectrum for the 42 V motor with different gate resistance. 37
4-15 Measurement result and Class 5 limit. 39

5-1 The π filter. 42
5-2 The T filter. 43
5-3 The L filter. 44
5-4 Line current waveform for a typical PWM drive with a resistive load. 45
5-5 Two types of damping circuit. 47
5-6 Equivalent circuits for (a) capacitors, and (b) inductors. 48
5-7 Usable frequency ranges for various types of capacitors. 49
5-8 Insertion loss of the EMI filter. 50

6-1 Test bench layout with the EMI filter. 52
6-2 EMI level before modification. 53
6-3 LC loop formed by the parasitic components of the Schottky diode and the wiring. 54
6-4 EMI level after modification. 55

A-1 Insertion loss definition. 60
A-2 Voltages and currents definition for a two-port network. 60

List of Tables

2.1 Minimum scan time. 13
2.2 Measuring instrument bandwidth (6 dB.) 14
2.3 Conducted emission limits. 15

4.1 Current waveform parameters for different loads. 31
4.2 Current waveform parameters for different gate resistance. 36

Chapter 1

Introduction

1.1 Why PWM Control?

To make driving a safer, more comfortable, and more exciting experience, automobile designers keep including electronic devices into their designs, which require higher power from the power supply. Increased awareness of environmental issues has resulted in demands for substantial improvements in fuel efficiency in today's automobiles. These demands become a great challenge in future automobile designs. The current 14 V system, however, has a very difficult time meeting this challenge economically. A solution to this problem is a new 14 V/42 V dual-voltage system [1].

With a 42 V power supply available, alternative ways of operating existing devices, e.g., various dc motors and lamps, can greatly improve the performance of such devices. One appealing example is to use pulse-width modulated (PWM) control to manipulate the operation of the motors and lamps. Not only does PWM control improve the controllability and efficiency of such devices, but it also allows automobile designers to easily accommodate new features in their design, e.g., varying the speed of dc motors or adjusting the brightness of lamps. Power MOSFETs are ideal for such applications, and they are more economical at 42 V than at 14 V in many aspects.

1.2 Research Objectives

While semiconductor based PWM motor drives bring many advantages, they introduce electrical noise to the surrounding environment which can cause operational failures of other

electronic devices, e.g., ECUs and radio receivers [2]. Usually an EMI filter is required to suppress this unwanted noise. A good understanding of the electrical characteristics of the PWM motor drives, especially their electromagnetic interference (EMI) behavior, can significantly reduce the cost of EMI filter design [3]. In the mean time, no standard exists for the 42 V electrical system, and what levels of conducted emission should be expected from such a system are not very clear. Therefore, some accurate EMI measurements on the PWM motor drives and a thorough analysis of these measurement results are invaluable for both the EMI designers and those who establish the standard.

The objectives of this research project are to:

1. Predict the EMI behavior of a typical PWM dc motor drive used in automotive applications through theoretical calculations;

2. Conduct a series of EMI measurements with a prototype PWM dc motor drive under various load conditions and electrical parameters;

3. Analyze the measurement results and comparing them with the theoretical calculations;

4. Develop a simple and effective EMI filter design methodology for this particular application.

1.3 Thesis Organization

The project is divided into several different stages, and the thesis is organized in chapters accordingly. The content of each chapter is described briefly below.

The second chapter conducts a theoretical calculation for the noise emission of PWM motor drives. It also defines EMI/EMC and provides some background knowledge of EMI/EMC classification and EMI standards adopted by the automotive industry.

The third chapter describes a measurement test setup specified by the EMI standard, and describes each functional unit in the setup. Schematics of important functional units, such as the prototype PWM motor drive and the Line Impedance Stabilization Network (LISN) are shown.

The fourth chapter presents EMI measurement results for a prototype PWM dc motor drive under various load conditions and electrical parameters along with a detailed analysis

of these results. The measurement is conducted without any filter element in the circuit. The measured EMI level is then compared to the existing standard, and the insertion loss required to meet the standard is calculated.

The fifth chapter describes several most common EMI filter topologies and their advantages and disadvantages. constraints on EMI filter design for this particular application are listed. A simple and reliable EMI filter design method will be presented.

The sixth chapter presents EMI measurement results with the EMI filter inserted into the system. Necessary modifications for improving the performance of the filter are discussed.

The last chapter presents conclusions and recommendations for future work.

Chapter 2

Theoretical Background

Electromagnetic Interference (EMI) is a problem that exists in all electrical systems. All electrical circuits emit electrical noise while operating. If not controlled properly, the noise can affect the normal operation of other devices, or even destroy them, through common electrical connections or electromagnetic coupling. The issue of compatibility among electrical devices in a system or common environment has evolved into an engineering discipline, *Electromagnetic Compatibility*, or EMC. EMC is an engineering discipline that investigates the amount of electrical noise that different devices can generate or tolerate, and establishes standards to provide limits on the amount of noise different devices should generate or be able to tolerate, in order to have them work together in a system or a common environment [2].

EMC has two interrelated aspects associated with it: emission and immunity. Emission

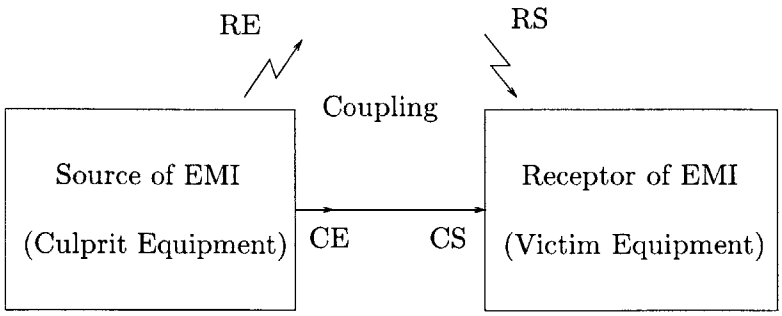

Figure 2-1: EMC/EMI overview. RE – radiated emission.
RS – radiation susceptibility. CE – conducted emission.
CS – conduction susceptibility.

deals with how much noise emitted by each of the devices in a common environment should be allowed such that the total noise existing in the environment is not fatal for the normal operation of any individual device. Immunity is concerned with how much noise a device should be able to withstand before it malfunctions.

In this chapter, characteristics of the noise generated by a PWM drive circuit will be examined and basic background knowledge of EMI will be provided.

2.1 EMI Calculation for a PWM dc Motor Drive

The characteristic impedance of the wiring used in automotive applications varies with frequency due to its parasitic inductances and capacitances. At frequencies below 100 kHz, the characteristic impedance is below 5 Ω. At frequencies above 100 kHz, the impedance is nearly a constant 50 Ω [2]. The wiring can be modeled as a transmission line.

In PWM dc motor drive applications, power flowing from the source to its load is controlled by turning an electrical switch on and off with different duty ratios at a frequency of a few kHz or higher. During switching, fast current transitions occur on the load side of the transmission line, and these fast current transitions create two types of noise. The first type, the conducted noise, affects other devices through common electrical connections and the second type, the radiated noise, through electromagnetic coupling.

In the first case, frequency harmonics of the fast switching current propagate back to the source, and cause voltage ripple and spikes on the output of the power supply.

In the second case, the fast switching current generates high voltage spikes across the ends of the transmission line. This is a result of the fast current transition and the parasitic inductance of the transmission line. Suppose that the line inductance L_{line} and current $i_{line}(t)$ are known, the voltage across the transmission line, v_{line}, during switching can be calculated according to the relationship $v_{line} = L_{line}(di_{line}(t)/dt)$. Even though the transmission line inductance is usually very small, i.e., on the order of several μH for automotive applications, v_{line} can be quite high during a very short period of time. Due to the frequency content of these large voltage spikes, energy will radiate into the surrounding environment in the form of electromagnetic waves.

Characteristics of noise emission for a PWM dc motor drive can be best understood through its power spectrum in the frequency domain. Since the power spectrum can not be

measured directly, the voltage spectrum is usually used instead. The power spectrum can then be deduced from the voltage spectrum.

Figure 2-2 approximates the line current waveform of a PWM motor drive circuit with resistive or highly inductive loads. A is the amplitude of the waveform. T is the period, R,

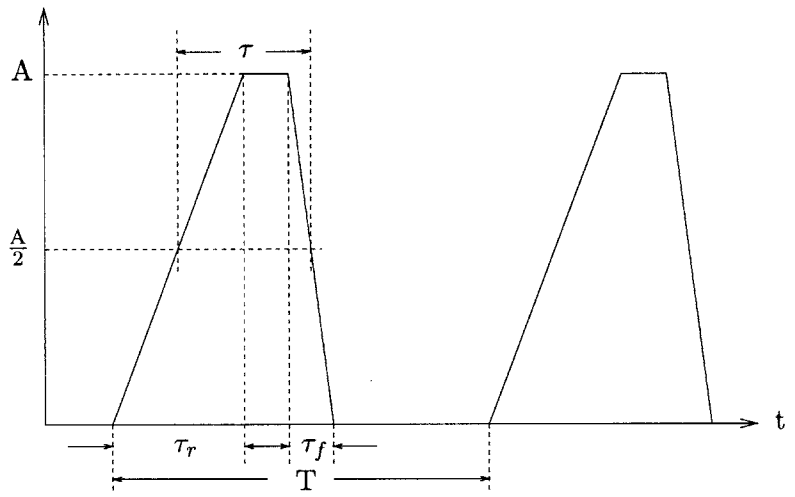

Figure 2-2: Line current waveform for a typical PWM drive with a resistive load.

F, and d are the relative rise time, the relative fall time and the duty ratio, respectively. The variables R, F, d are related to T by the following expressions:

$$\begin{aligned} R &= \tau_r/T, \quad \text{relative rise time,} \\ F &= \tau_f/T, \quad \text{relative fall time,} \\ d &= \tau/T, \quad \text{duty ratio,} \end{aligned} \tag{2.1}$$

with the constraints

$$d + \frac{R+F}{2} \leqslant 1 \quad \text{and} \quad \frac{R+F}{2} \leqslant d. \tag{2.2}$$

Since the duty ratio varies much slower in time than the switching frequency, it is assumed to be a constant in the calculation.

The spectrum of this current waveform can be derived through Fourier analysis [4]. Since the current waveform is periodic, its spectrum has nonzero values only at discrete frequencies, e.g., dc, the switching frequency and its higher harmonics. The harmonics for the switching frequency can be expressed in terms of the harmonic number, k, as $f_k = kf_{sw}$, where f_{sw} is the switching frequency, and f_k is its kth harmonic. Given the time domain

signal is $s(t)$, its Fourier transform, expressed in terms of k, is

$$S(k) = \frac{A}{\pi k}(\text{ sinc } (\pi kR)\ e^{j\pi kd} \ - \ \text{sinc } (\pi kF)\ e^{-j\pi kd}), \tag{2.3}$$

where sinc $(x) = \sin\ (x)/x$.

The amplitude spectrum of the waveform shown in Fig. 2-2 is plotted in Fig. 2-3 for the following set of parameters: $A = 1/\sqrt{2}$ A, R =.008, F =.01, d =.2, and f_{sw} =20 kHz. The envelope shown in the figure, described in the next paragraph, tracks the local maxima of the waveform tightly. Frequency spectrum analysis shows that the energy level of the noise

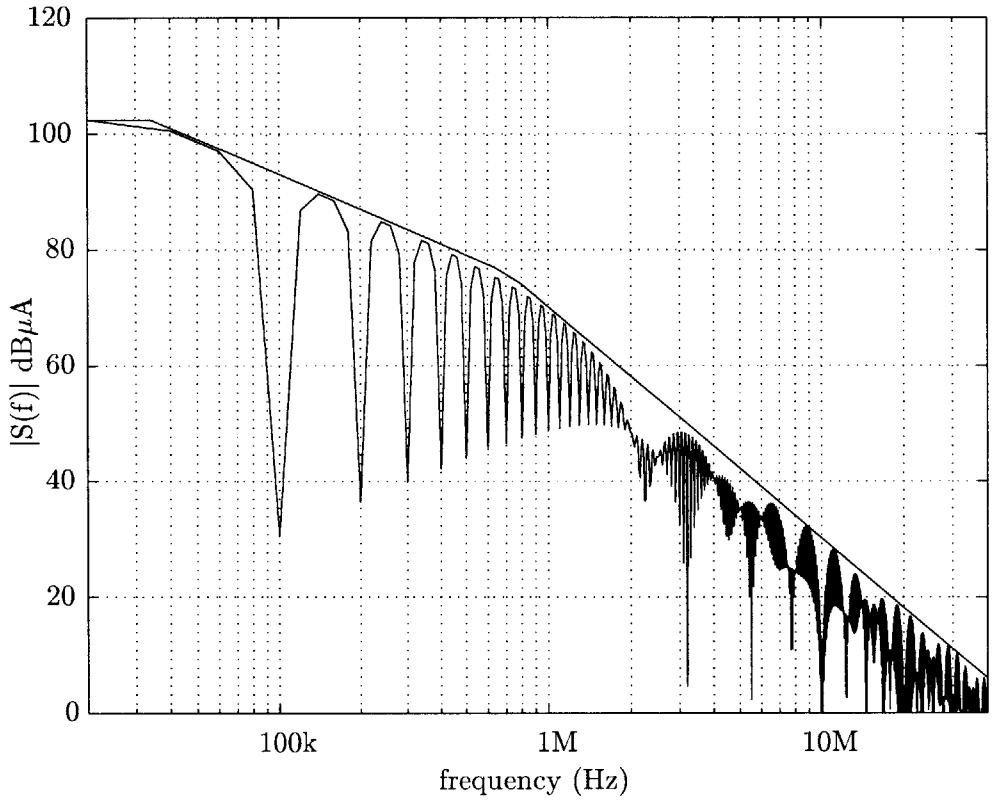

Figure 2-3: Calculated spectrum for a typical PWM drive input current.

concentrates at the switching frequency and its low harmonics. The energy level decreases rapidly as frequency increases [4]. Other parameters, such as duty ratio, rise time and fall time, determine the shape of the envelope.

The envelope of the spectrum can be divided into four segments. For low frequencies, i.e., between the switching frequency and the first cutoff harmonic, the segment is a constant

and is equal to the amplitude spectrum magnitude at the switching frequency, that is

$$|S(f_{sw})| = \frac{A}{\pi}\sqrt{(\text{sinc}\,(\pi R) + \text{sinc}\,(\pi F))^2 \sin^2(\pi d) \;+\; (\text{sinc}\,(\pi R) - \text{sinc}\,(\pi F))^2 \cos^2(\pi d)}. \tag{2.4}$$

The first cutoff harmonic is

$$k_1 = \frac{2}{\sqrt{(\text{sinc}\,(\pi R) + \text{sinc}\,(\pi F))^2 \sin^2(\pi d) \;+\; (\text{sinc}\,(\pi R) - \text{sinc}\,(\pi F))^2 \cos^2(\pi d)}}. \tag{2.5}$$

For frequencies at which $\text{sinc}\,(\pi k R) \approx \text{sinc}\,(\pi k F) \approx 1$, the segment is linear and it can be expressed as

$$|S(f_l)| = \frac{2A}{\pi k}. \tag{2.6}$$

This expression is valid between the first and the second cutoff harmonics. The second cutoff harmonic is

$$k_2 = \frac{1}{\pi\alpha}, \quad \alpha = \begin{cases} R & \text{if } R > F \\ F & \text{if } R < F. \end{cases} \tag{2.7}$$

Between the second and the third cutoff harmonics, the segment is

$$|S(f_m)| = \frac{A}{\pi k}\left(1 + \frac{1}{\pi k \alpha}\right), \quad \alpha = \begin{cases} R & \text{if } R > F \\ F & \text{if } R < F. \end{cases} \tag{2.8}$$

The third cutoff harmonic is

$$k_3 = \frac{1}{\pi\beta}, \quad \beta = \begin{cases} F & \text{if } R > F \\ R & \text{if } R < F. \end{cases} \tag{2.9}$$

For frequencies above f_{k_3}, where $|\,\text{sinc}\,(\pi k R)\,| \leqslant |\,1/\pi k R\,|$ and $|\,\text{sinc}\,(\pi k F)\,| \leqslant |\,1/\pi k F\,|$, the segment is also linear, and it is expressed as

$$|S(f_h)| = \frac{A}{\pi^2 k^2}\left(\frac{1}{R} + \frac{1}{F}\right). \tag{2.10}$$

Since the envelope of the spectrum covers all local maxima very tightly, it can represent the upper bound of the spectrum. Not only are the cutoff harmonics and the segments of the envelope easier to calculate than the spectrum, but the envelope also gives much insight on how the spectrum changes as waveform parameters vary.

When R and F are much less than 1, (which is generally true for current waveforms of PWM dc motor drives), the four major factors affecting the spectrum distribution of the noise are R, F, d and A. The duty ratio only influences the first cutoff frequency f_{k_1} and the amplitude for frequencies lower than f_{k_1}. The other two cutoff frequencies solely depend on R and F.

For frequencies less than the first cutoff frequencies f_{k_1}, $|S(f_{sw})|$ is proportional to $A/sin(\pi d)$.

For frequencies between f_{k_1} and the second cutoff frequency f_{k_2}, the spectrum is proportional to A.

For frequencies between f_{k_2} and f_{k_3}, the spectrum is roughly proportional to the ratio between A and α, because the product $\pi k\alpha$ is usually much less than 1. The definition for α is given in Eq. 2.7.

For frequencies higher than f_{k_3}, the spectrum depends on all three factors, A, R and F. If A, R and F increase by the same factor, the magnitude of the spectrum will not change. When one of R and F is much smaller than the other, the larger one can be ignored. In another words, the spectrum in this frequency range depends on A and β, with β as defined in Eq. 2.9.

These interesting conclusions will be used to analyze the EMI measurement result presented in Chapter 4.

2.2 EMI Classification

To better understand and describe EMI disturbances, it is beneficial to specify and classify EMI noise in terms of its electrical characteristics. This, however, is not an easy task. EMI can be classified in terms of its frequency content and its transmission mode [2].

2.2.1 Classification by Frequency Content

There are many methods to classify EMI disturbances by its frequency content. Most of these methods are used in transmission line EMI analysis and filter design for power transmission, and they are irrelevant for applications considered here. Only the broadband and narrowband classifications are worth mentioning, since they determine the resolution bandwidth used in the measurement.

The noise components in a system are usually very complex due to the fact that there are many individual noise sources in the system emitting noise with different characteristics. Circuits utilizing oscillators to generate sinusoidal waveforms at a single frequency as an operational necessity create noise with a very narrow bandwidth, perhaps less than 1 Hz. This kind of noise is defined as narrowband. Circuits generating fast switching waveforms, such as switched-mode power supplies, or PWM motor drives, create noise with frequency components spreading over tens or hundreds of megahertz. This kind of signal is broadband [5].

2.2.2 Classification by Transmission Mode

EMI can be classified as conducted and radiated EMI in terms of the medium through which it propagates [3]. The conducted EMI propagates through metal wiring and other conductive parts, i.e., heat sinks or the ground plane. The radiated EMI propagates through air and it affects other devices through electromagnetic coupling.

Conducted noise can be further classified as differential mode (or symmetrical) and common mode (or asymmetrical) in terms of the conduction path it takes. In Fig. 2-4, I_d represents the differential mode current, and I_c represents the common mode current. v_{noise}

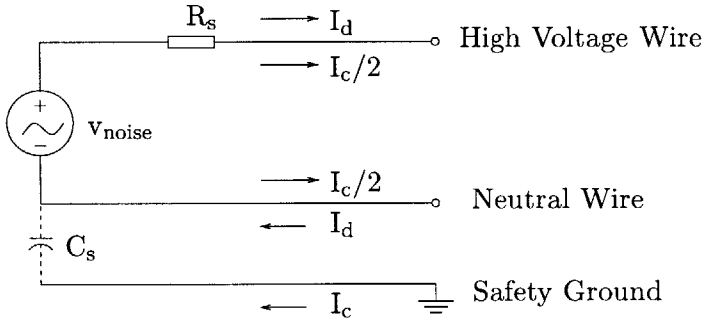

Figure 2-4: Differential mode and common mode current.

is the noise source. Differential mode current flows out of the noise source through the high voltage wire and returns to the source from the neutral wire. Common mode current flows out of the noise source through both the high voltage wire and the neutral wire, and returns to the source through the safety ground.

In automotive applications, a separate safety ground path does not exist. When a device

is directly mounted onto the car body, the car body acts as the neutral wire. When a device is isolated from the car body, twisted pair wires are used to connect it to the power supply, and no local grounding is provided. For this reason, the common mode noise will not be considered in this investigation.

For industrial and household applications, the EMI measurement is generally conducted in two frequency bands, 0.15 MHz to 30 MHz, and 30 MHz to 300 MHz, according to the transmission mode of the noise. For automotive applications, the two frequency bands are from 150 kHz to 108 MHz, and from 150 kHz to 960 MHz. For different transmission modes, different measurement methods apply. Detailed descriptions of the standards for automotive applications are presented in Section 2.5.

2.3 Investigation and Reduction of Conducted EMI

The switching frequency for PWM dc motor drive applications is a few kilohertz up to several tens of kHz. According to Fig. 2-3, most of the noise energy is concentrated at the fundamental switching frequency and its immediate higher harmonics. At such low frequencies, almost all of the electrical energy will be in the form of conducted emission, because the relatively short wiring used in automobile applications prevent electrical signals at these frequencies to radiate efficiently.

The level of the radiated EMI depends on the level of the conducted EMI in all frequency ranges. Furthermore, reducing the radiated EMI requires such expensive steps as building higher quality shielding boxes, and using expensive co-axial cables. Consequently, it is much cheaper to reduce the radiated EMI by first eliminating the conducted EMI as much as possible. So, reducing the conducted EMI before trying to reduce the radiated EMI is a common practice.

Because of the time constraints on this research project and the reasons listed above, the investigation will focus on the reduction of differential mode conducted EMI in PWM motor drives.

2.4 Definition of Insertion Loss

The performance of an EMI filter is measured in terms of insertion loss. Insertion loss of a filter is defined as the ratio of the powers consumed by the load in a reference circuit before

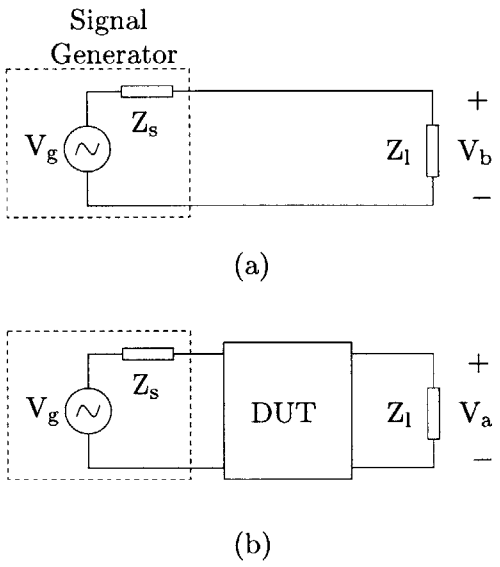

Figure 2-5: Insertion loss definition. (a) Reference circuit. (b) Test item inserted.

and after the filter is inserted into the reference circuit (Fig. 2-5). It can be expressed as

$$\begin{aligned} IL &= 10 \log\left(\frac{P_b}{P_a}\right) \\ &= 20 \log\left(\frac{V_b}{V_a}\right) \end{aligned} \tag{2.11}$$

where P_b and P_a correspond to the power dissipated by the load before and after the filter is inserted, and V_b and V_a are the corresponding voltages across the load. In practice, the reference circuit has identical source and load impedance, i.e., $Z_l = Z_s$.

If the Z parameters or the A parameters for the filter are known, the insertion loss of the filter can be expressed in terms of these parameters as

$$\begin{aligned} IL &= 20 \log\left|\frac{(Z_{11}+Z_s)(Z_l+Z_{22})-Z_{12}Z_{21}}{(Z_s+Z_l)Z_{21}}\right| \\ &= 20 \log\left|\frac{A_{11}Z_l+A_{12}+A_{21}Z_sZ_l+A_{22}Z_s}{Z_s+Z_l}\right|. \end{aligned} \tag{2.12}$$

(Please see Appendix A for the derivation of Eq. 2.12.) The Z parameters and the A

parameters are defined as

$$\begin{pmatrix} V_1 \\ V_2 \end{pmatrix} = \begin{pmatrix} Z_{11} & Z_{12} \\ Z_{21} & Z_{22} \end{pmatrix} \begin{pmatrix} I_1 \\ I_2 \end{pmatrix}$$
$$\begin{pmatrix} V_1 \\ I_1 \end{pmatrix} = \begin{pmatrix} A_{11} & A_{12} \\ A_{21} & A_{22} \end{pmatrix} \begin{pmatrix} V_2 \\ -I_2 \end{pmatrix}. \tag{2.13}$$

The voltage and current signals V_1, I_1, V_2 and I_2 are defined in Fig. A-2. Insertion loss is different from attenuation in the sense that it is determined not only by the characteristics of the circuit, but also by the source and load impedances.

2.5 Standard SAE J1113/41

Due to the nature of their operating environment, different types of applications require different EMI limits; therefore, various EMI standards exist. For the automotive industry, all electronic devices installed in cars sold in the United State should meet standard SAE J1113/41.

Standard SAE J1113/41 provides details of test requirements and guidelines. Requirements are imposed on such things as power supply, measurement resolution bandwidth, ground noise level, ground plane and test layout. Requirements on resolution bandwidth and ground noise level are given in this section, and the rest will be given in the next chapter.

Table 2.1 and Table 2.2 give minimum scan time and measurement instrument bandwidth required for the measurement.

Table 2.1: Minimum scan time [6].

Band	Peak Detection	Quasi-peak Detection
9-150 kHz	Does not apply	Does not apply
0.15-30 MHz	100 ms/MHz	200 s/MHz
30-1000 MHz	1 ms/MHz or 100 ms/MHz[1]	20 s/MHz

[1] When 9 kHz bandwidth is used, the 100 ms/MHz value shall be used.

The frequency range specified in SAE J1113/41 is different from that specified in stan-

Table 2.2: Measuring instrument bandwidth (6 dB.)

Frequency Band		Broadband Peak and Quasi-peak	Narrowband Peak and Average
0.15-30 MHz		9 kHz	9 kHz
30-1000 MHz	FM Broadcast	120 kHz	120 kHz
30-1000 MHz	Mobile Service	120 kHz	9 kHz

dards applied in industrial and household appliances. According to SAE J1113/41, the frequency range of interest for the conducted EMI is from 150 kHz to 108 MHz and that of the radiated EMI is in the range from 150 kHz to 960 MHz.

Table 2.3 provides the limits on conducted emission for peak and quasi-peak detection. The limits are divided into classes. The ground noise level for EMI measurement should be at least 6 dB below the limit specified by the test plan. When designing the filter, the proper limit will be chosen according to the design specifications, and the difference between this limit and the measurement results is the insertion loss needed.

Table 2.3: SAE J1113/41 limits for broadband conducted disturbances on power input terminals (peak or quasi-peak detector) [6].

(a) Peak detector.

Class	Levels in dB ($dB\mu V$) .15-.3 (MHz)	Levels in dB ($dB\mu V$) .53-2.0 (MHz)	Levels in dB ($dB\mu V$) 5.9-6.2 (MHz)	Levels in dB ($dB\mu V$) 30-54 (MHz)	Levels in dB ($dB\mu V$) 70-108 (MHz)
1	113	95	77	77	61
2	103	87	71	71	55
3	93	79	65	65	49
4	83	71	59	59	43
5	73	63	53	53	37

(b) Quasi-peak detector.

Class	Levels in dB ($dB\mu V$) .15-.3 (MHz)	Levels in dB ($dB\mu V$) .53-2.0 (MHz)	Levels in dB ($dB\mu V$) 5.9-6.2 (MHz)	Levels in dB ($dB\mu V$) 30-54 (MHz)	Levels in dB ($dB\mu V$) 70-108 (MHz)
1	100	82	64	64	48
2	90	74	58	58	42
3	80	66	52	52	36
4	70	58	46	46	30
5	60	50	40	40	24

Chapter 3

Experimental Setup

EMI measurement is a well know difficult task, because many factors can affect the credibility and repeatability of the measurement. For example, if equipment in the test setup is not carefully isolated electrically from the environment, additional paths for the noise signal may be introduced, and the measurement result may be higher or lower than the actual value. Another example would be that a very noisy environment would push the measurement result into an erroneously high level at some frequencies (this is particularly true for radiated EMI measurement). Because of the nature of this experiment, testing environment and equipment layout are considered very carefully.

3.1 Test Bench Layout

The test bench layout used in this experiment follows recommendations given by standard SAE J1113/41. Figure 3-1 shows the top view of the relative positions of the equipment on a common ground plane. The common ground plane is made with a $8' \times 3' \times 1/8'$ brass plate.

The ground plane is crucial for correct EMI measurement for two reasons. Not only is it a reference point with respect to which the noise spectrum is measured, but it also serves as a shielding of the test equipment against ambient noise.

For differential mode noise measurement, all of the equipment is electrically floating with respect to the brass plate, except the Line Impedance Stabilization Network (LISN.) The ground terminal of the LISN is connected to the brass plate. The electrical isolation is created by lifting all devices 40 mm from the ground plane. The following sections will

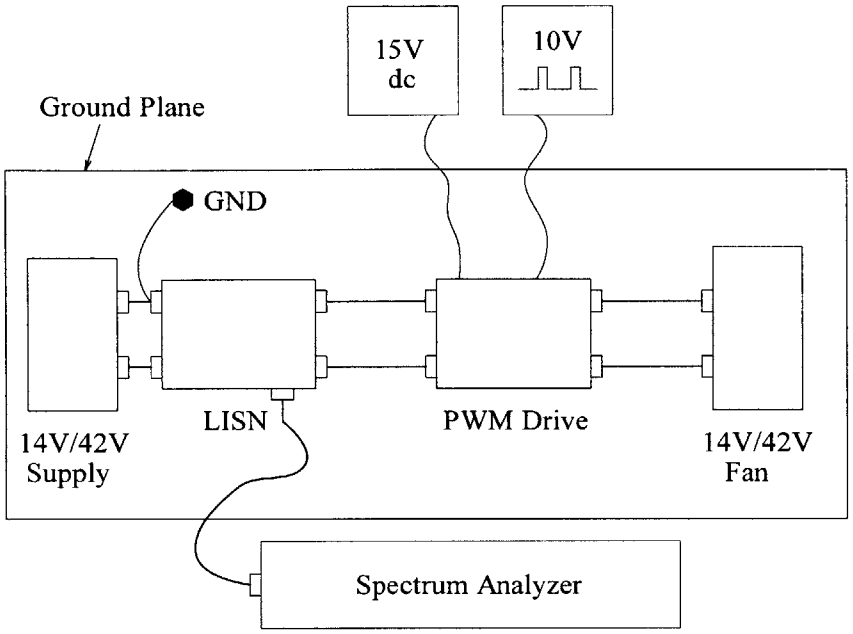

Figure 3-1: Test bench layout for EMI measurement.

describe the functionality of each unit.

3.2 Loads

Loads used for the measurement are two dc blower-fan motors supplied by Daimler-Chrysler. One is rated for 14 V, and the other for 42 V. Both of them are regular brushed dc motors with maximum power ratings of 140 W. The original EMI filters installed in the two motors are disconnected before the measurement, because these filters will lower the noise level and affect the accuracy of the measurement.

3.3 PWM Motor Drive Circuit

Fig. 3-2 shows the schematic for the prototype PWM dc motor drive designed for this experiment. The IR2125 is a MOSFET gate driver IC from International Rectifier. This chip is capable of both high-side and low-side switching.

For a power rating of 140 W, the maximum current that will flow in this circuit with a 14 V power supply is 10 A. The highest supply voltage used in this experiment is 42 V. To meet these two requirements, an N-channel enhancement-mode MOSFET transistor,

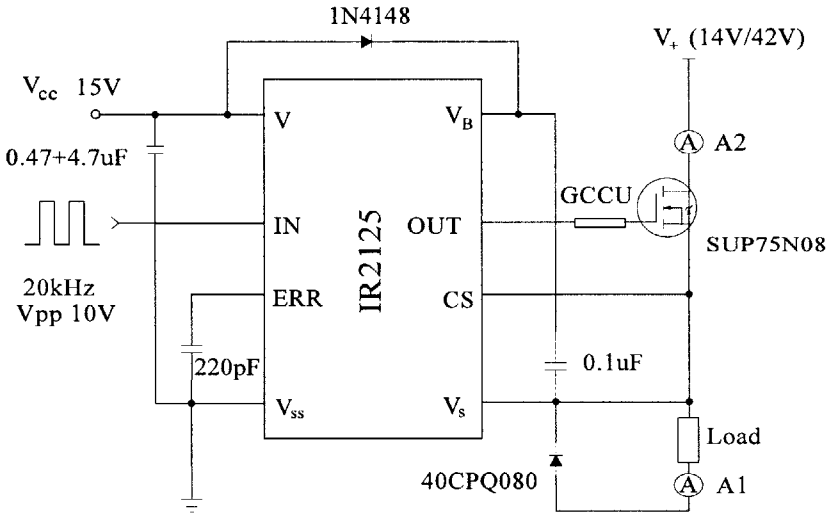

(a)

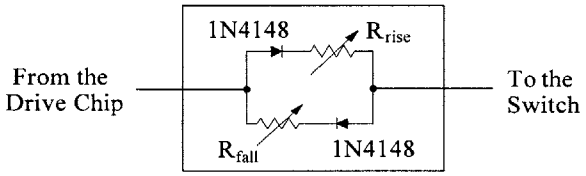

GCCU (Gate Current control Unit)

(b)

Figure 3-2: (a) PWM dc motor drive circuit diagram. (b) Gate Current Control Unit (GCCU).

SUP75N08 by Temic Semiconductors, is used. High-side switching is adopted in this experiment.

The IR2125 utilizes the bootstrap method to control the gate of the MOSFET to achieve high-side switching. When the control signal is low, the capacitor between V_B and V_S, C_{boot}, is charged up by the dc power supply connected to V_{CC}. The voltage of this dc power supply should be between 10 V and 20 V. When the input signal is high, V_B and OUT are connected inside the IR2125, and the current flows from C_{boot} to the gate of the MOSFET through V_B and OUT. The switch starts to conduct once the gate-source voltage V_{gs} reaches its threshold voltage, and it will remain conducting as long as V_{gs} is sufficiently high. Capacitor C_{boot} has to be large enough to keep V_{gs} greater than the threshold voltage during the time the switch is on.

A Schottky diode, 40CPQ080, connected across the inductive load provides a path for the load current to prevent instantaneous current changes in the load when the MOSFET is turned on and off.

The Gate Current Control Unit (GCCU) between the output pin of the IR2125 and the gate of the MOSFET switch controls the rise and fall time during switching. The rise and fall time directly influences the di/dt level of the current waveform, and consequently, it affects the energy distribution of the noise in the frequency domain. A more detailed description of the GCCU can be found in Chapter 4.

3.4 Rectangular Wave Generator and Power Supplies

The control signal of the IR2125 is provided by a rectangular wave generator with a variable duty ratio and switching frequency. This rectangular wave generator is designed and built around a LM555 one-shot timer IC from National Semiconductor, and the schematic of the circuit is shown in Fig. 3-3.

The timing parameters can be determined by the following equations:

$$t_{high} = 0.67(R_A) \cdot C_C \tag{3.1}$$

$$t_{low} = 0.67(R_B) \cdot C_C \tag{3.2}$$

$$T = t_{high} + t_{low} \tag{3.3}$$

$$D = \frac{t_{high}}{T} \tag{3.4}$$

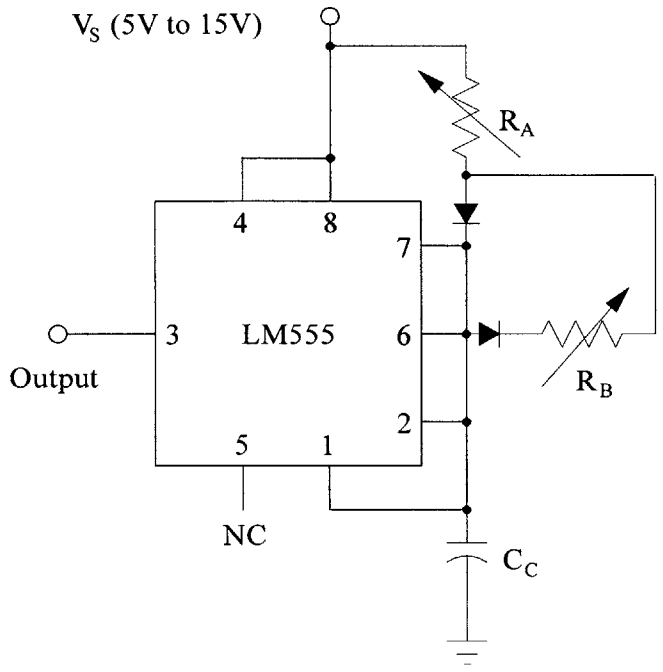

Figure 3-3: Rectangular wave generator.

The capacitor C_C is chosen to be 220 pF, and R_A and R_B are 1 MΩ potentiometers. With these components, the duty ratio can be easily adjusted from 1% to 99% for a 20 kHz switching frequency.

The main power supply should be able to handle at least 45 V and 20 A. Since the intention of the first phase of this experiment is to measure the noise generated by the PWM motor drive and its load, no EMI filter is used. Without EMI filters, the voltage ripple on the output of the power supply is large enough such that the IR2125 and the LM555 will not function properly if they share the same power supply as the rest of the circuit. Therefore, a separate dc supply is needed for the IR2125 and the LM555 chip. A regular car battery became a natural candidate for this purpose.

An ac/dc power supply and a function generator may replace the car battery and the rectangular wave generator, if they do not affect the EMI measurement in any significant way by introducing additional pathes for the EMI noise. A pair of twisted wires should be used for connection between each of these two devices and the PWM circuit to minimize the differential mode noise bypassed through them. Experiments have been done with this alternative, and no significant difference is observed.

3.5 LISN

One of the major factors making EMI measurement a difficult task is that the impedance of the power supply is usually unknown, or varying in a wide range as a function of time. To make the measurement reliable and repeatable, a Line Impedance Stabilization Network (LISN) is always inserted between the source and the device under test (DUT). The functionality of the LISN is less intuitive than other units in the test setup, but it should become clear by the end of this section.

Figure 3-4 shows a typical circuit diagram for LISN. Three major functionalities of the

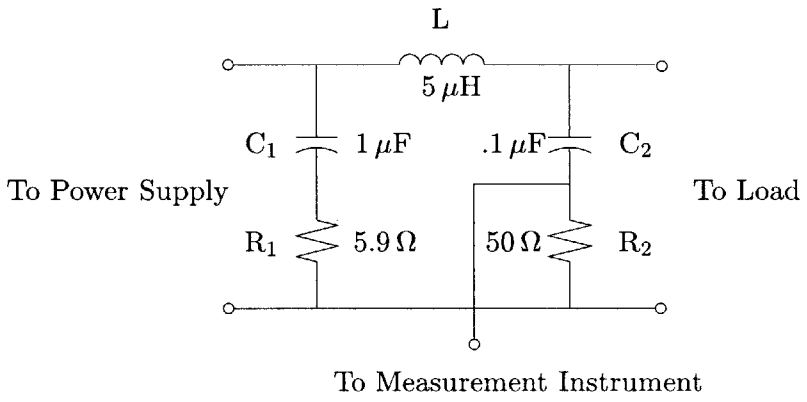

Figure 3-4: Line Impedance Stabilization Network (LISN).

LISN are:

1. To create an artificial transmission line impedance for the load;
2. To prevent the EMI noise from flowing back to the power supply and affecting its proper operation;
3. To provide a measurement outlet for the noise measurement instrument.

At low frequencies, i.e., the switching frequency of the PWM drive and its first several harmonics, the two capacitors, C_1 and C_2, have high impedances, and the inductor is virtually a short. The LISN is transparent between the power supply and its load (Fig. 3-5(a)). At high frequencies, where the specifications are given, the LISN acts as an open circuit between the power supply and the load because of the inductor (Fig. 3-5(b)). The measurement is taken across the 50 Ω resistor on the load side of the LISN, which is equal to

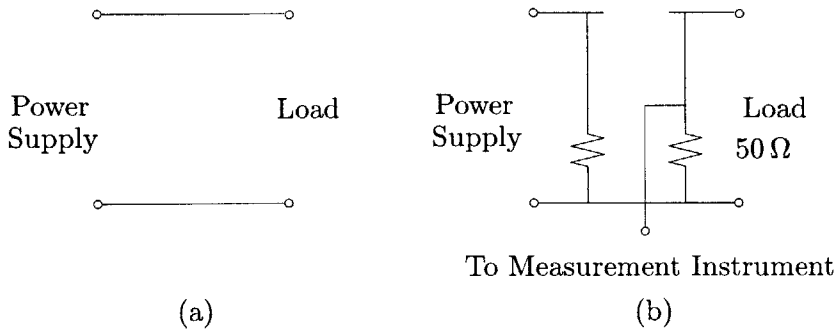

Figure 3-5: LISN equivalent circuit. (a) Low frequency. (b) High frequency.

the characteristic impedance of the wiring seen by the noise source at high frequencies. The impedance looking into the load side of the LISN can be measured or calculated by shorting the two terminals on the supply side. The calculated load side impedance of the LISN for the frequency range between 100 kHz and 30 MHz is given in Fig. 3-6. The calculated and measured insertion loss of the LISN in the same frequency range is given in Fig. 3-7.

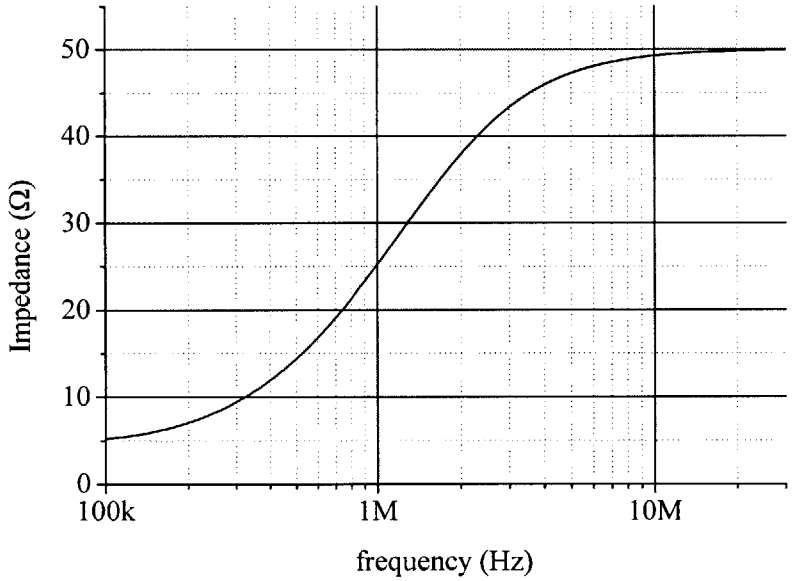

Figure 3-6: Calculated load side impedance of the LISN.

The load side impedance model developed here, along with the current spectrum formulated in Chapter 2, will be used to calculate the voltage spectrum of the noise in the next chapter.

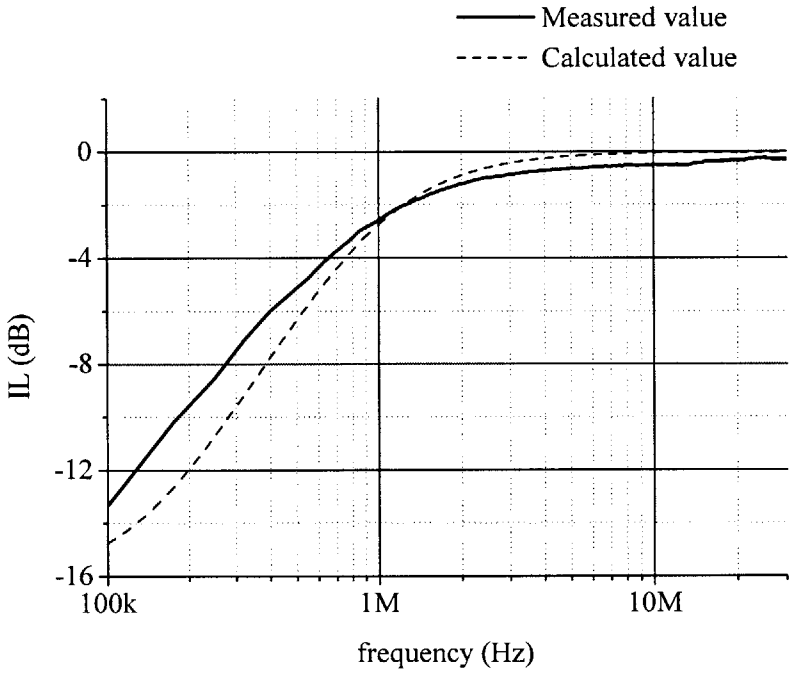

Figure 3-7: Measured and calculated insertion loss of the LISN.

Chapter 4

EMI Measurement without EMI Filter

This chapter shows EMI measurement results without the presence of the EMI filter. Both the frequency and time domain measurements are recorded and a detailed analysis is provided. The test setup was described in Chapter 3.

The following questions will be answered with the measurement results presented in this chapter:

1. What level of EMI emission should be expected in the frequency range of specification for both the 14 V system and the 42 V system;
2. How accurate is the theoretical model for the EMI emission developed in Chapter 2;
3. What are the key factors in determining the level of EMI emission;
4. Will a higher voltage power supply help to reduce conducted EMI;
5. What effects does the gate resistance have on the level of conducted EMI;
6. How much attenuation does an EMI filter need to meet the EMI limits of standard SAE J1113/41 for the 42 V load?

To answer these questions, both the 14 V and 42 V dc motors are used. Different electrical parameters, i.e., duty ratio and gate resistance, are utilized.

4.1 EMI Measurement under Different Load Conditions

Although the PWM dc motor drive is rarely used in the current 14 V electrical system, EMI measurements under this voltage will be extremely helpful for a general understanding of electrical noise generation. These measurements can also help to answer whether any improvement, in terms of conducted emission, can be expected by increasing the source voltage from 14 V to 42 V, as commonly anticipated.

The switching frequency is chosen to be 20 kHz for two major reasons. The first reason is that if the switching frequency is lower than 20 kHz, the mechanical part of the system will produce acoustic noise audible to humans. The second reason is that by setting the switching frequency as low as possible, the energy content of its harmonics in the frequency range of interest can be minimized, which, in turn, lowers the insertion loss requirement for the EMI filter to meet the specification. The lower insertion loss needed, the smaller the filter elements required, and therefore, the cheaper the filter becomes.

The test setup is shown in Fig. 3-1. The duty ratios of the control signal are set to 50%, 30% and 20% for the measurement. The average current level is expected to decrease as duty ratio decreases while other conditions are the same.

4.1.1 Time Domain Measurement for the 42 V Motor

Figures 4-1, 4-2 and 4-3 plot the control signal and the line current for the 42 V load at duty ratios of 50%, 30% and 20%, respectively. One important observation is that the ratio between the overshoot and the amplitude of the current waveform increases significantly as the duty ratio decreases, which corresponds to an increase in the di/dt level. The significance of the di/dt level will be discussed in Section 4.1.3.

Figure 4-4 shows the voltage waveform across the EMI measurement output on the LISN at 50% duty ratio. This plot covers two switching periods. The high voltage spikes are induced by current pulses through the capacitor on the load side of the LISN during switch on and off. These voltage spikes are the source of the noise and are to be eliminated by the EMI filter. Figure 4-5 shows the voltage waveform across the terminals on the load side of the LISN, and Figure 4-6 shows the voltage waveform across the terminals on the power supply side of the LISN, both for 50% duty ratio.

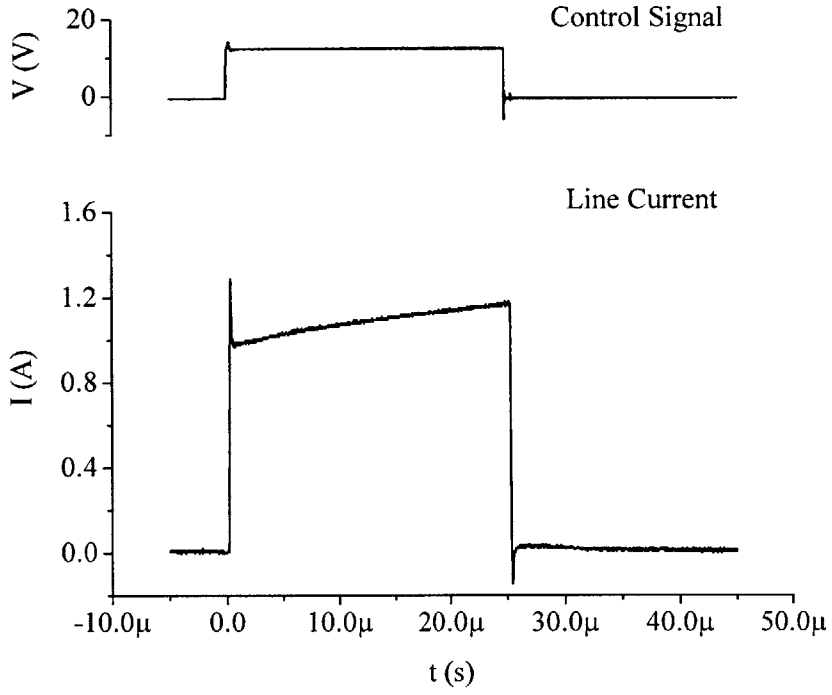

Figure 4-1: Control signal and line current for 50% duty ratio.

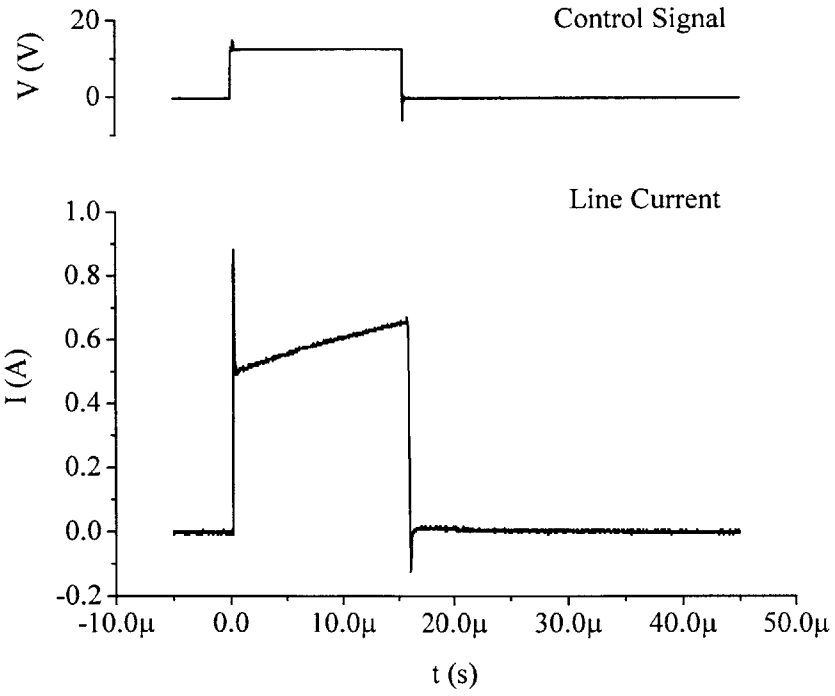

Figure 4-2: Control signal and line current for 30% duty ratio.

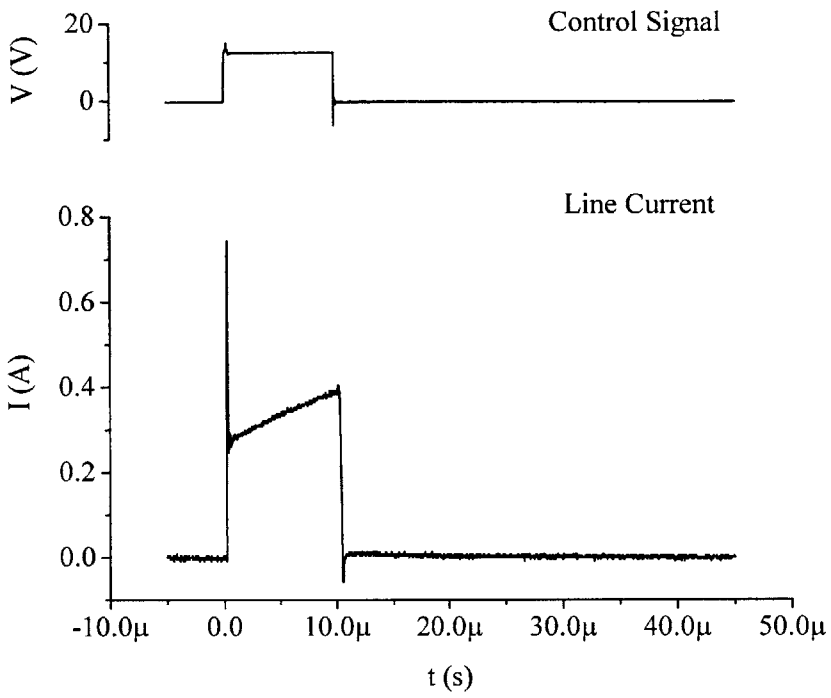

Figure 4-3: Control signal and line current for 20% duty ratio.

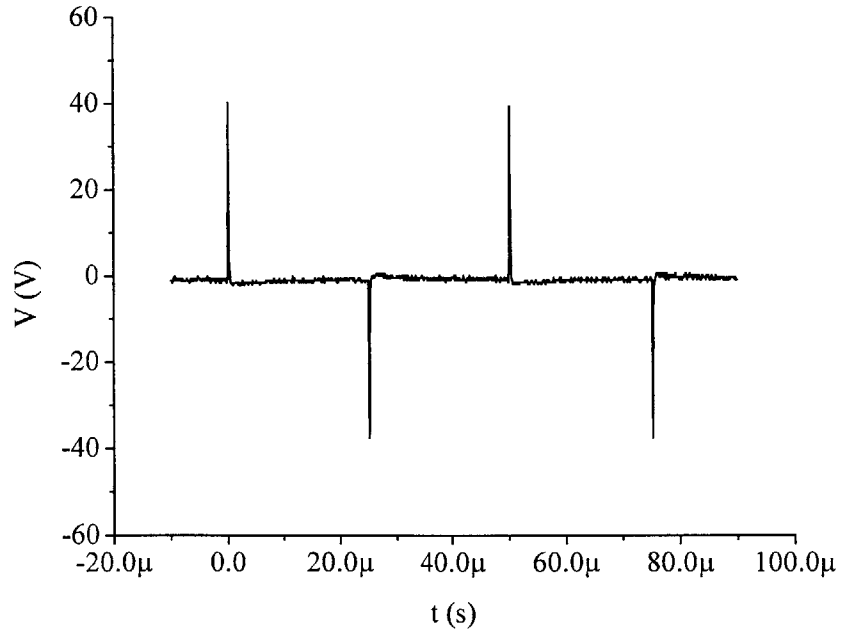

Figure 4-4: Voltage across the EMI measurement output on the LISN.

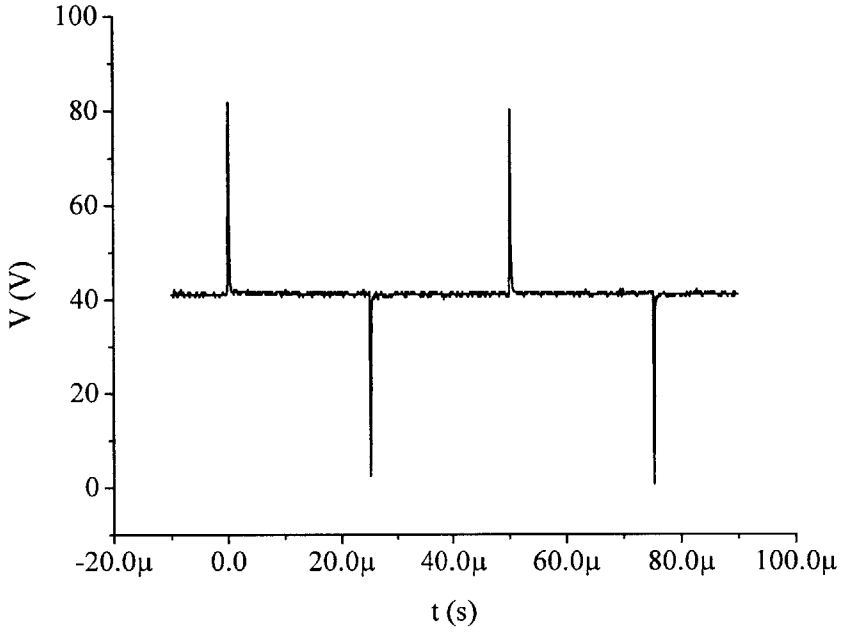

Figure 4-5: Voltage across the load side of the LISN.

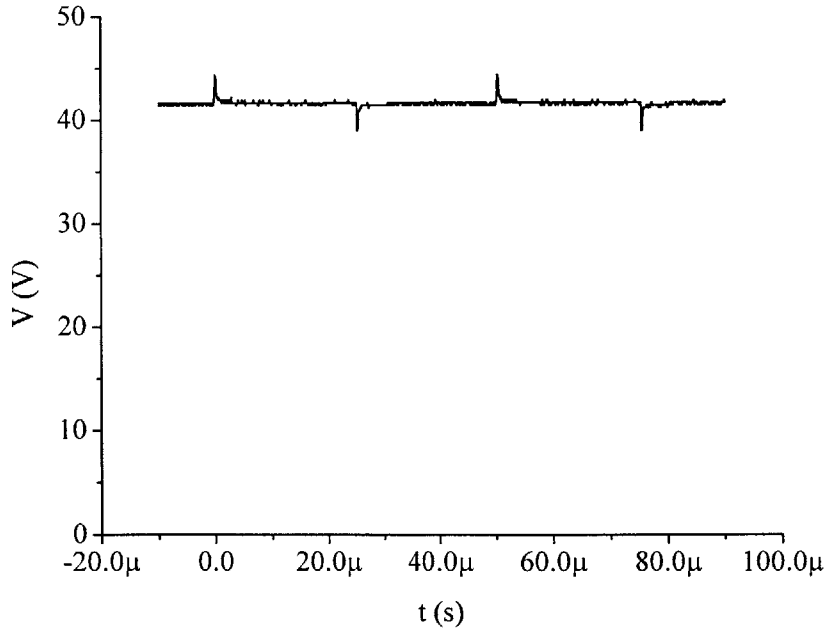

Figure 4-6: Voltage across the power supply side of the LISN.

4.1.2 Time Domain Measurement for the 14 V Motor

This section shows control signal and line current records for the 14 V motor. The average current level for the 14 V motor is two to three times higher than the average current level for the 42 V motor for the corresponding duty ratio. Comparing with current waveforms of the 42 V motor, the overshoot level for the 14 V motor is significantly lower. The relative magnitude of the current overshoot for the 14 V load is much smaller than that for the 42 V load. This implies that the theoretical calculation derived in Chapter 2 will be more accurate for the 14 V load than for the 42 V load, because the current waveform for the 14 V load is much closer to the trapezoidal approximation.

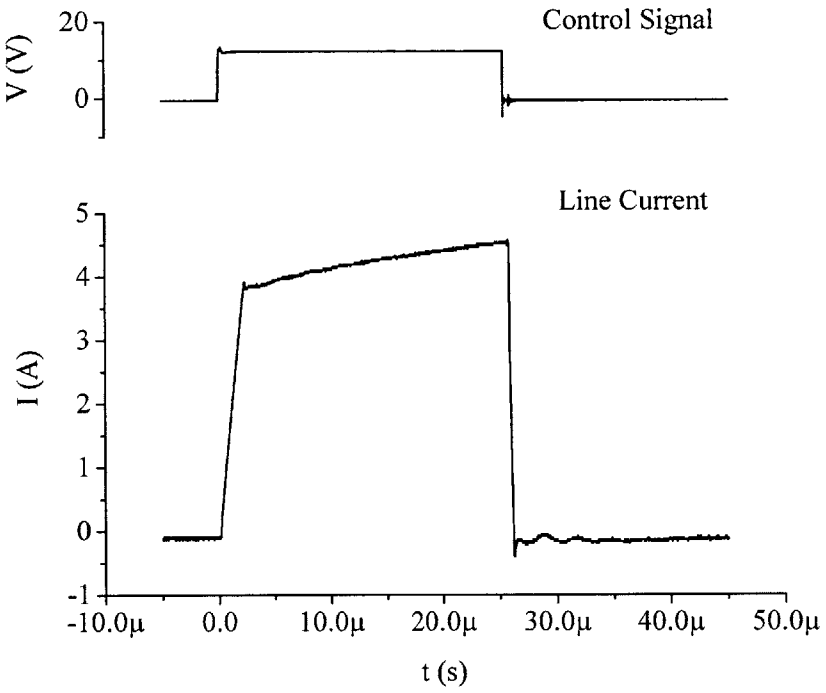

Figure 4-7: Control signal and line current for 50% duty ratio.

Table 4.1 summarizes the di/dt level and the amplitude of the current waveforms shown in this section. With these di/dt values, the relative rise time, R, and the relative fall time, F, for each waveform can be calculated. For any duty ratio, both the amplitudes and the β values (defined in Eq. 2.9) are roughly three times higher for the 14 V load than for the 42 V.

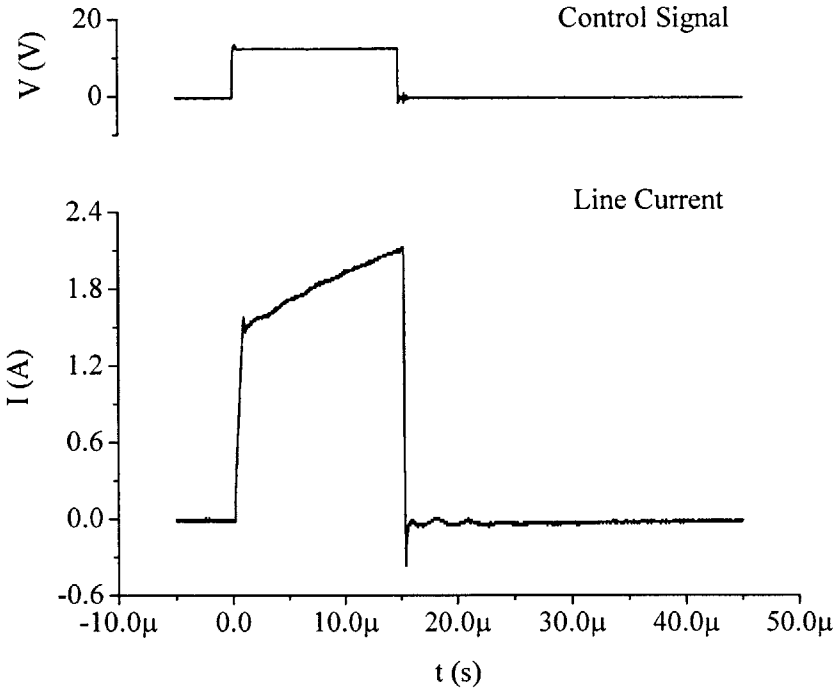

Figure 4-8: Control signal and line current for 30% duty ratio.

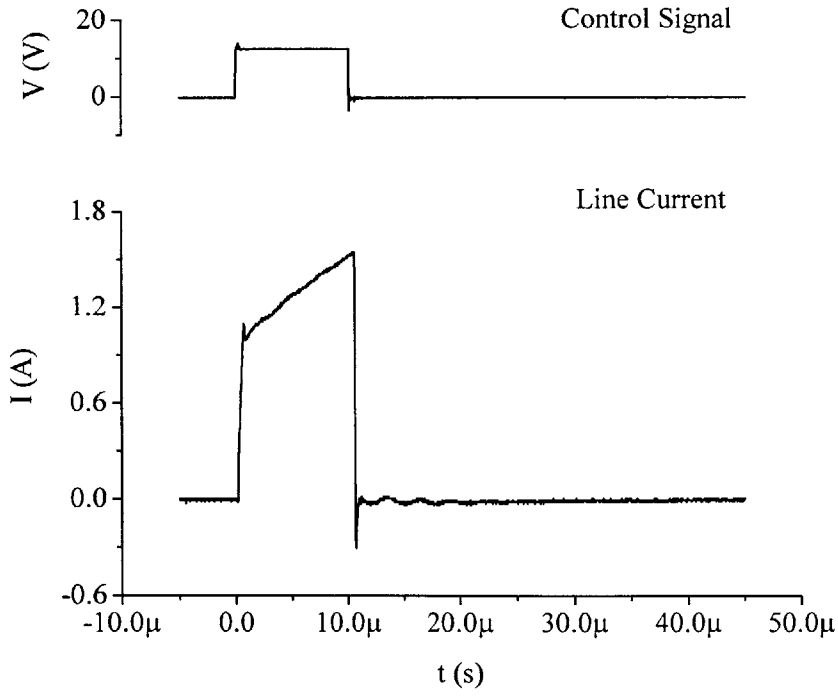

Figure 4-9: Control signal and line current for 20% duty ratio.

Table 4.1: Current waveform parameters for different loads.

	Duty ratio	$di(t_{rise})/dt$ (A/μs)	$di(t_{fall})/dt$ (A/μs)	Amplitude (A)
42 V	50%	11.2	8.95	1.20
	30%	15.9	4.62	.628
	20%	17.2	2.47	.442
14 V	50%	1.87	11.9	4.50
	30%	1.99	16.1	2.03
	20%	2.30	22.1	1.33

4.1.3 Frequency Domain Measurement for Both Motors

The frequency spectrum of the noise can be easily calculated with theoretical results developed in Chapter 2. Fig. 4-10 shows the ac circuit model for the spectrum calculation, where

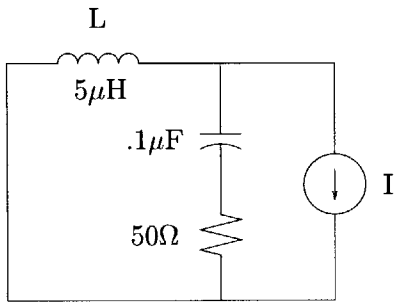

Figure 4-10: The ac circuit model for the measurement circuit. The PWM drive with its load is modeled as a current source.

the PWM drive circuit and its load is replaced by a current source. The dc power supply is shorted for ac calculation. The calculation is incorrect for frequencies above 30 MHz, because the resolution bandwidth used in this frequency range is much higher than the switching frequency. The correct spectrum can be obtained by convolving an appropriate window with the calculated spectrum.

Figure 4-11 shows the calculated and measured spectrums for the 14 V load at 20% duty ratio. Current parameters used in the calculation are A =1.33 A, R =.01, F =.0012, d =.2, and f_{sw} = 20 kHz, which are obtained from Table 4.1. These parameters were defined in Section 2.1. The two curves follow each other closely.

Different from the case for the 14 V load, the calculated spectrum for the 42 V load

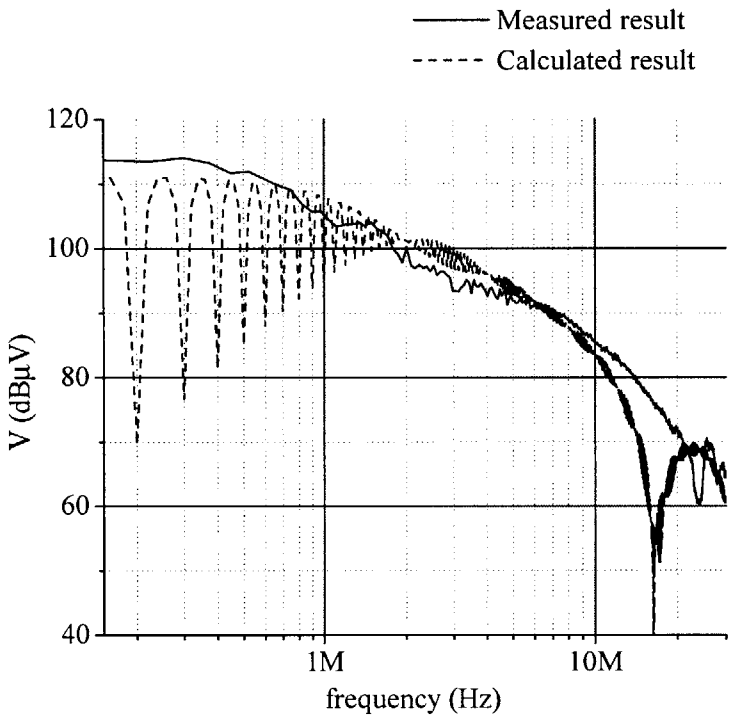

Figure 4-11: Measured and calculated noise frequency spectrum for the 14 V load with 20% duty ratio from 150 kHz to 30 MHz.

follows the measured result nicely at frequencies between 150 kHz and 1 MHz, but deviates upward at higher frequencies. This is due to the overshoot that exists in the line current for the 42 V load. The calculated spectrum for the 42 V load is not shown here.

As mentioned in Section 2.5, different resolution bandwidths should be applied to different frequency ranges. Since the PWM drive circuit emits broadband noise, a 9 kHz resolution bandwidth is chosen for the frequency range from 150 kHz to 30 MHz , and 120 kHz for the frequency range from 30 MHz to 108 MHz. The frequency domain measurement results are shown in Figures 4-12 and 4-13, corresponding to the two frequency ranges given above. Another requirement for correct EMI measurement is that the ambient noise level should be at least 6 dB lower than the limit specified in the test plan. The ground noise level is shown in Fig. 4-14, and it does satisfy the requirement for meeting the Class 5 limit defined in Table 2.3.

The theoretical analysis in Chapter 2 concludes that when R and F are much smaller than the switching period, the spectrum distribution of the current waveform depends on three parameters, R, F and A. Furthermore, once A is fixed, R and F are determined by the di/dt level.

The current amplitude for the 42 V load is three times smaller than that for the 14 V load for the same duty ratio (shown in Table 4.1). The magnitude of the two corresponding spectrums at low frequencies, i.e. 150 kHz, differs by a factor of three. Since the β values differ by a factor of three for the 14 V load and the 42 V load, the spectrums at high frequencies are roughly the same for the two loads at the same duty ratio.

The measurement implies that for low frequencies, i.e., 150 kHz, the noise level is higher for the 14 V system. For higher frequencies, however, prediction will have to be made based on all important factors, especially, R and F. The measurement result shown in this section is consistent with the conclusion given in Chapter 2.

4.2 EMI Measurement with Different Gate Resistance

For reasons related to the nonideal properties of the filter components, it is often desirable to reduce EMI level at high frequencies, i.e., above 10 MHz. Since both the calculated and measured results predict that the β value, or equivalently, the di/dt level determines the EMI level at high frequencies, reducing the di/dt level can achieve the goal. One method

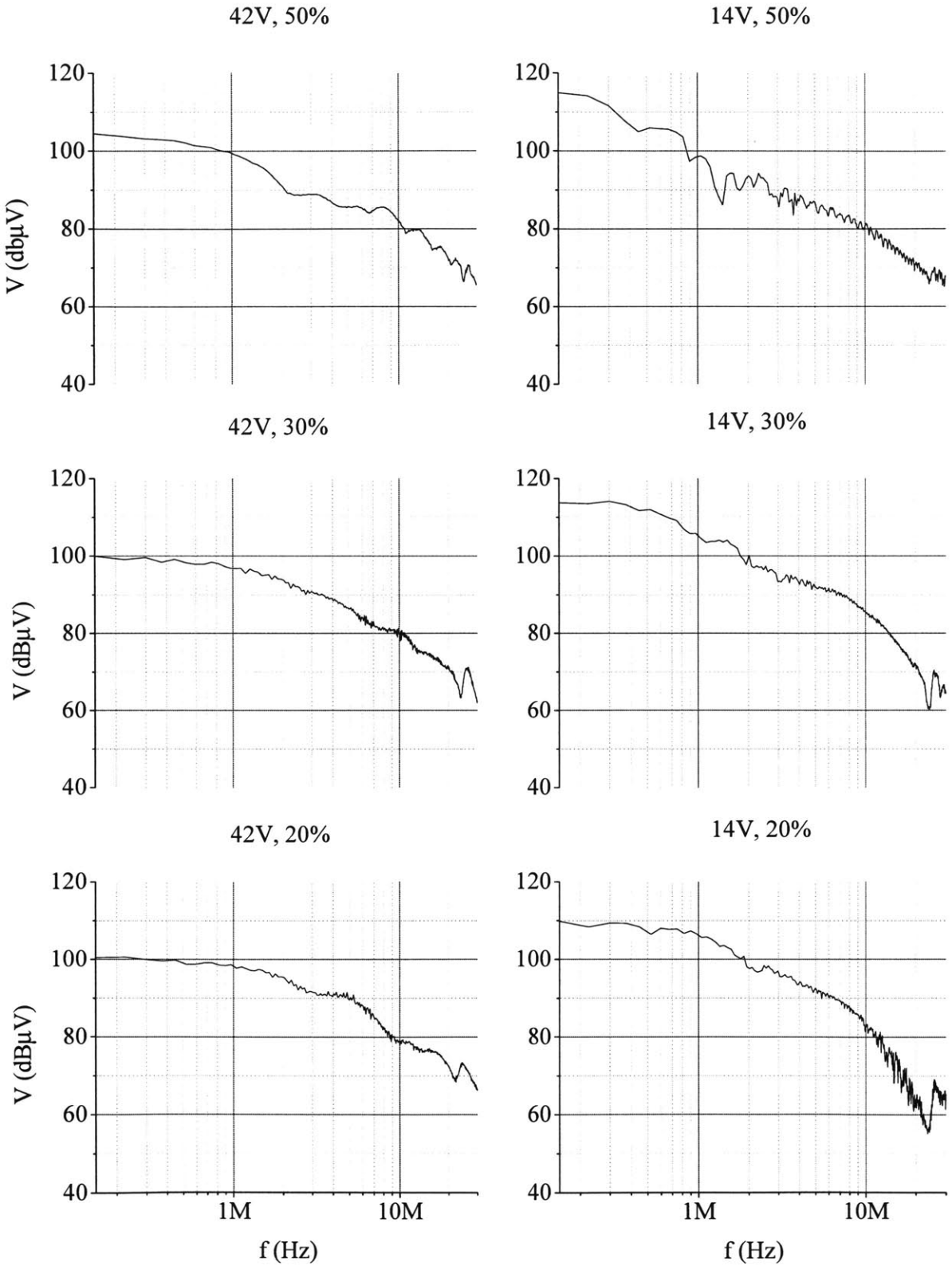

Figure 4-12: Spectrum measured from 150 kHz to 30 MHz. The 42 V load is shown on the left column and the 14 V load is shown on the right column. Duty ratio: 50%, 30% and 20%.

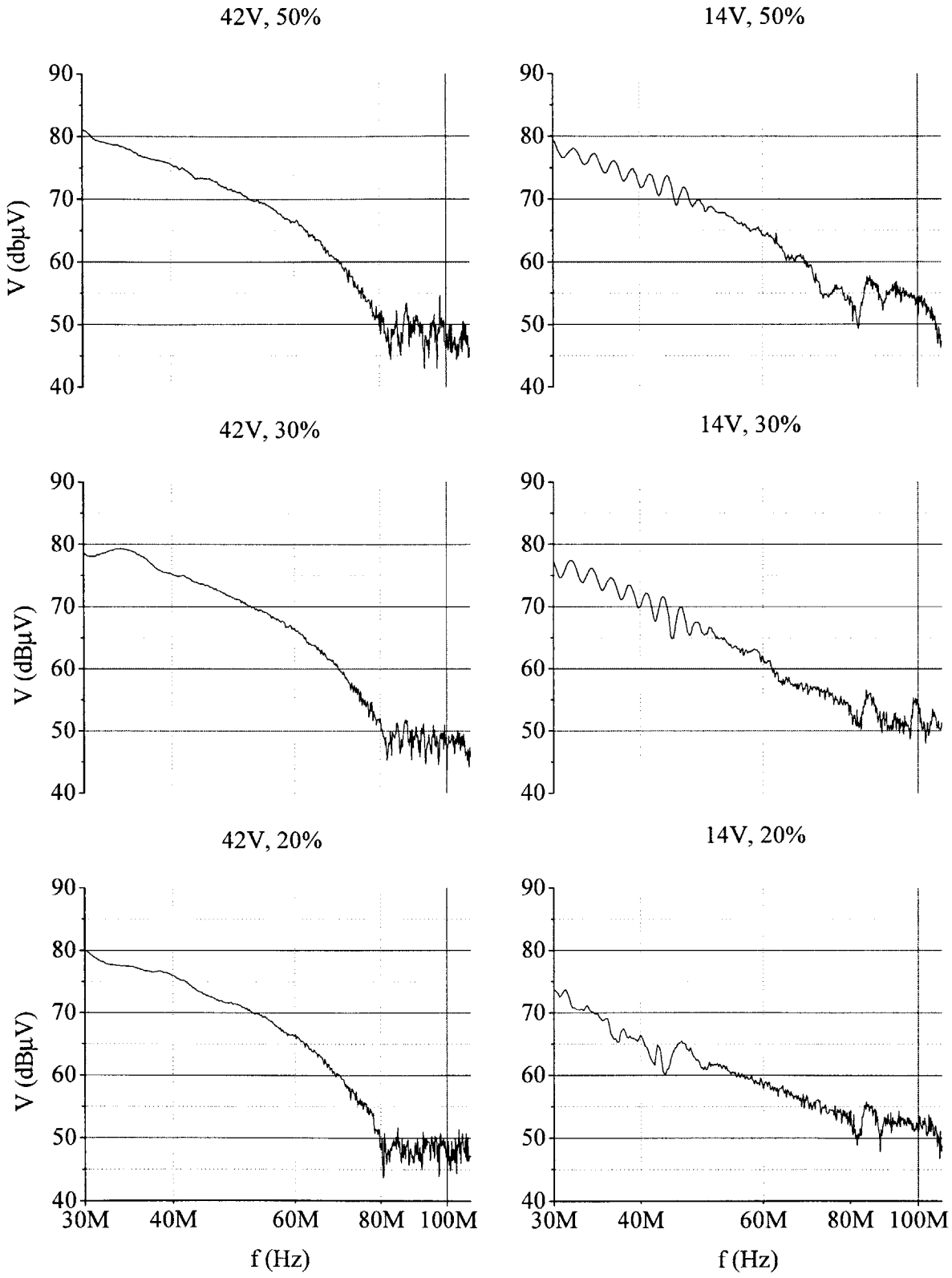

Figure 4-13: Spectrum measured from 30 MHz to 108 MHz. The 42 V load is shown on the left column and the 14 V load is shown on the right column. Duty ratio: 50%, 30% and 20%.

to lower the di/dt level is to increase the turn-on and turn-off time of the switch, which can be accomplished by increasing the gate resistance of the MOSFET switch.

This section will present EMI measurement results of the 42 V motor with different gate resistance. The gate resistance is controlled by the Gate Current Control Unit (GCCU). There are two separated paths for the gate current to flow through the GCCU, and each path is controlled by a diode. This structure of GCCU provides a way to control the rise time and the fall time individually, so that the difference in latencies for the rising edge and falling edge of the line current I_{in} is minimized, and the duty ratios for both I_{in} and the control signal are the same.

The di/dt levels of I_{in} for various pairs of gate resistance are measured and given in Table 4.2. Since only the greater di/dt value matters for high frequencies, one of the gate

Table 4.2: Current waveform parameters for different gate resistance.

Gate Resistance (Ω, Ω)	maximum $di(t_{rise})/dt$ (A/μs)	$di(t_{fall})/dt$ (A/μs)	Maximum di/dt (A/μs)	Amplitude (A)
(0, 0)	11.3	10.3	11.3	1.21
(84, 12)	6.75	8.88	8.88	1.14
(196, 29)	4.54	6.49	6.49	1.22
(1873, 337)	.928	2.65	2.65	1.077

resistors is set to get the desired maximum di/dt level, and the other is adjusted till the duty ratios of the current and the control signal are the same.

The measurement result in Fig. 4-14 shows that increasing the gate resistance indeed lowers the EMI level at high frequencies. The gate resistances used are listed above each plot. The bottom two plots are the ground noise and the noise generated by the rectangular wave generator. The emission level above 10 MHz eventually becomes lower than the noise generated by the rectangular waveform generator. The voltage amplitude also reduces as the gate resistance rises. For other considerations, e.g., switching loss, the gate resistance is usually less than 200 Ω.

4.3 Insertion Loss Requirement for the EMI Filter

Measurement results indicate that the EMI level increases as the duty ratio increases. Suppose that the maximum duty ratio will be applied to the circuit is 80%, the insertion loss

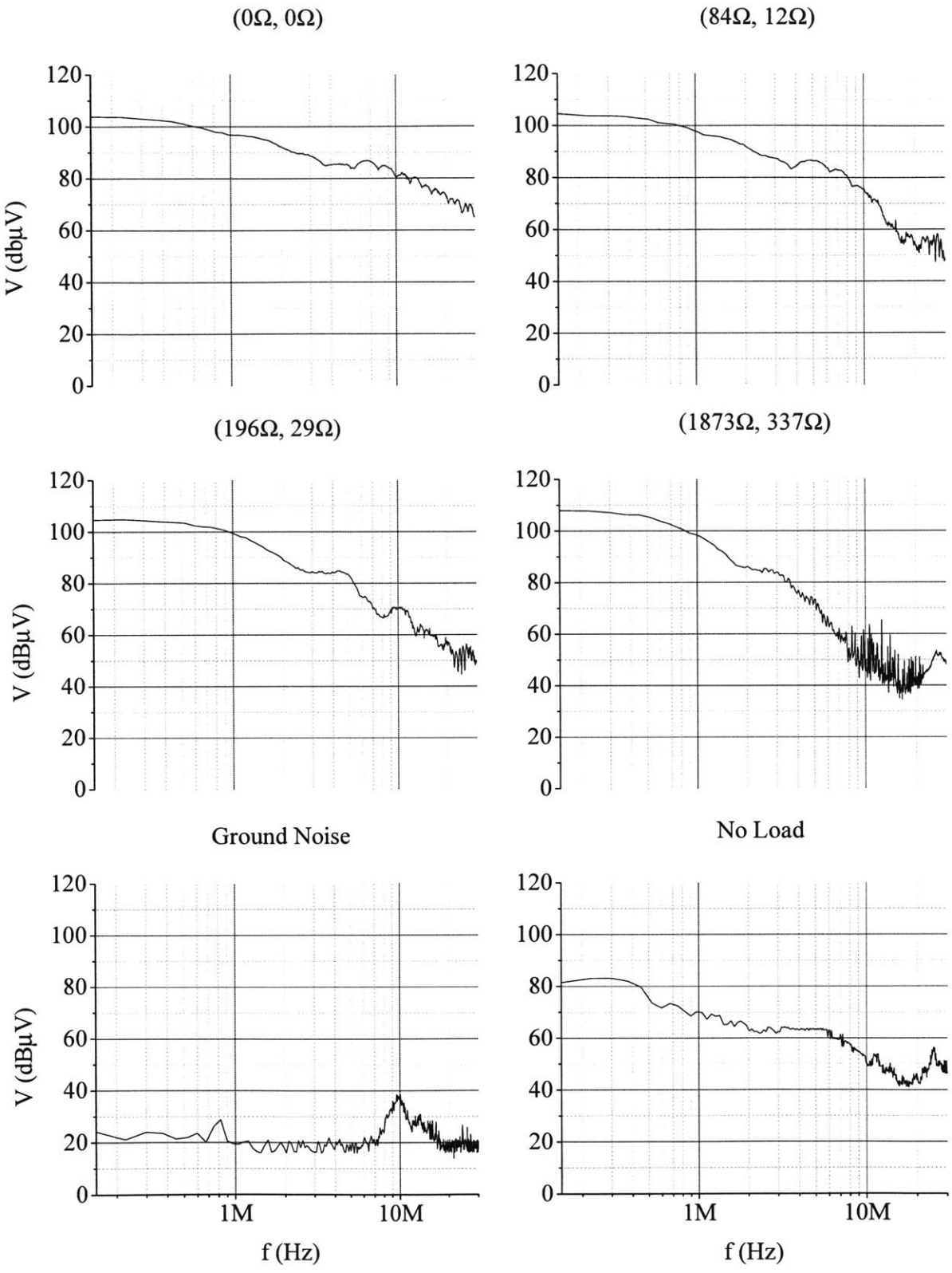

Figure 4-14: Spectrum for the 42 V motor with different gate resistance. Duty ratio is set to 50%. The gate resistance used are labeled as (R_{rise}, R_{fall}) on the top of each plot, where R_{rise} and R_{fall} are defined in Fig. 3-2.

needed to meet Class 5 limits in SAE J1113/41 is shown in Fig. 4-15. Class 5 limits are chosen because these are the limits set by the automotive industry for this application. The plot shows that the worst frequency is at 150 kHz, where 36 dB attenuation is needed to meet the Class 5 limit.

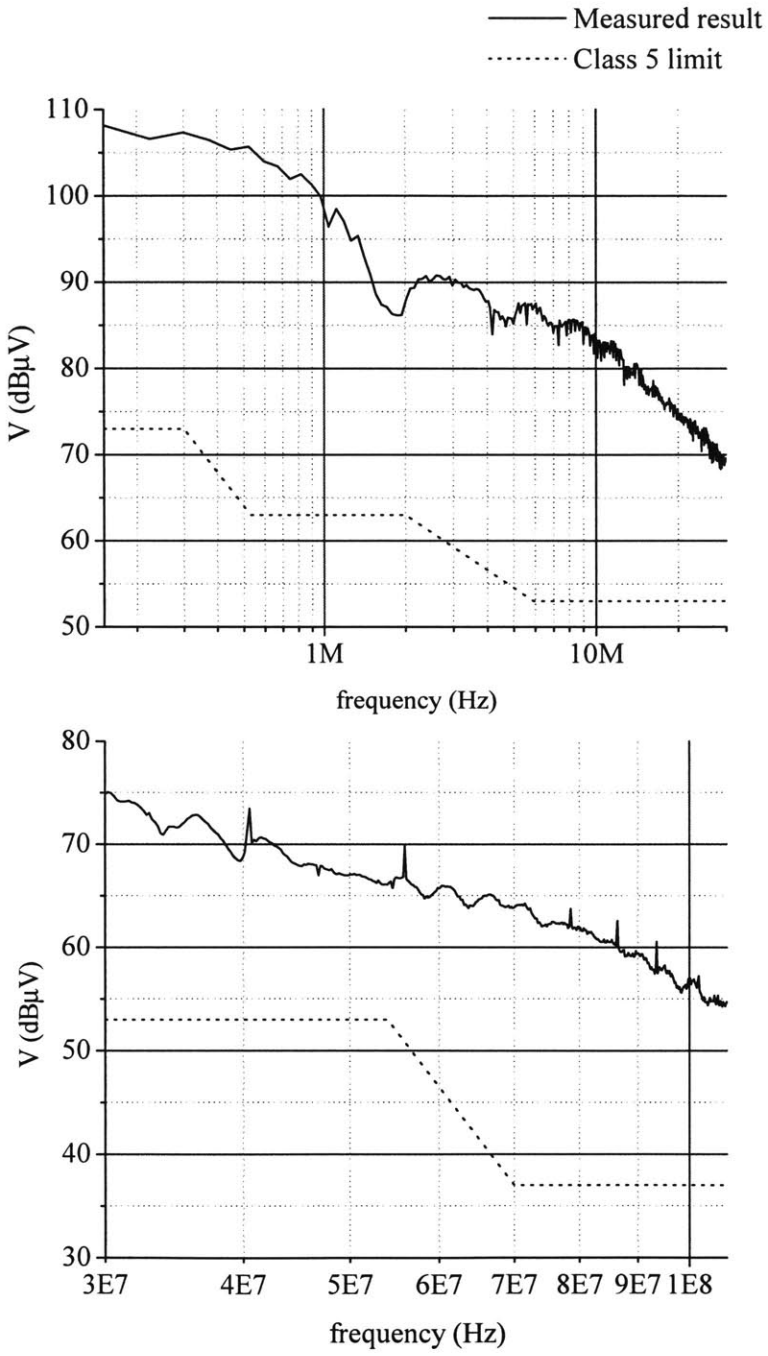

Figure 4-15: Measurement result and SAE J1113/41 Class 5 limits for the frequency range from 150 kHz to 30 MHz, and from 30 MHz to 108 MHz.

Chapter 5

EMI Filter Design

There are some fundamental differences between EMI filter design and conventional filter design. For conventional filter design, such as that used in communication, the input and output impedances are usually known. Specifications are often given on such parameters as ripple amplitudes in the pass band and stop band, as well as the transition width between the pass band and stop band. For an EMI filter, on the other hand, the performance is measured by the amount of insertion loss it can provide over its operating frequency range. Furthermore, EMI filters in general operate over a much wider frequency range than conventional filters do, and the flatness over the pass band or stop band is not a concern for EMI filters , as long as they can provide sufficient insertion loss over defined frequency ranges.

EMI filter design has often been called "Black Magic", both because EMI filter design criteria are so flexible that there is no standard design method adopted by filter designers, and because there are a great number of factors influencing the behavior of the filter. A designer will first determine the cutoff frequency and roll-off slope needed for the filter to meet the specifications. He will then choose a filter topology that satisfies these requirements, fix values of some of the components, and finally solve for the rest of the components. If one set of component values or one topology does not work, he will use a different set of components or topology. This process will continue till all of the components are reasonably chosen and all specifications are met. Such a process is a relatively difficult task for an inexperienced designer. Furthermore, it does not guarantee that the design is optimal in terms of the cost and volume of the filter.

This chapter will introduce some of the most popular EMI filter topologies, and discuss the advantages and disadvantages of each topology. Constraints on filter design for this particular type of applications will be addressed. These constraints will help to shrink down the design scope and make the filter design a much easier task.

5.1 EMI Filter Topologies

EMI filters, like other kinds of filters, are impedance mismatch devices. At low frequencies, or its pass band, the EMI filter is "transparent" between the source and the load. At high frequencies, where the specifications are given, it provides insertion loss by mismatching the source and load impedances. From the EMI point of view, the load is the noise source and the power supply is the victim that is to be protected. For reasons of convenience and clarity, the term "source" will be used to represent the power supply, and "load" to represent the noise source (the PWM drive). The insertion loss provided by the filter will eliminate harmful EMI noise flowing from the load to the source. The most popular differential mode EMI filter topologies are the π filter, the T filter and the L filter, and they are described in detail in the following sections.

5.1.1 The π Filter

The π filter is a third order filter (Fig. 5-1). Each of its elements provides 6 dB per octave, or 20 dB per decade decay. A one-stage π filter provides 18 dB per octave decay in total. Multiple stages of π filters can be cascaded to provide greater loss. A two-stage π filter (Fig. 5-1(c)), for example, has five elements and it can provide a total of 30 dB per octave decay. The π filter can be easily balanced by placing half of the inductance on the high voltage line, and the other half on the return path, as shown in Fig. 5-1(b). A balanced filter is not required for dc applications, but it makes each inductor smaller, which might be beneficial for packaging.

The π filter works very well when the source and load impedances are high. When the source impedance is low, however, the value of the capacitor facing the source becomes very large in order to provide the roll-off slope required. For example, if the source has an output impedance of a 10 μF, the value of the capacitor, C, will have to be one order of magnitude greater, or 100 μF.

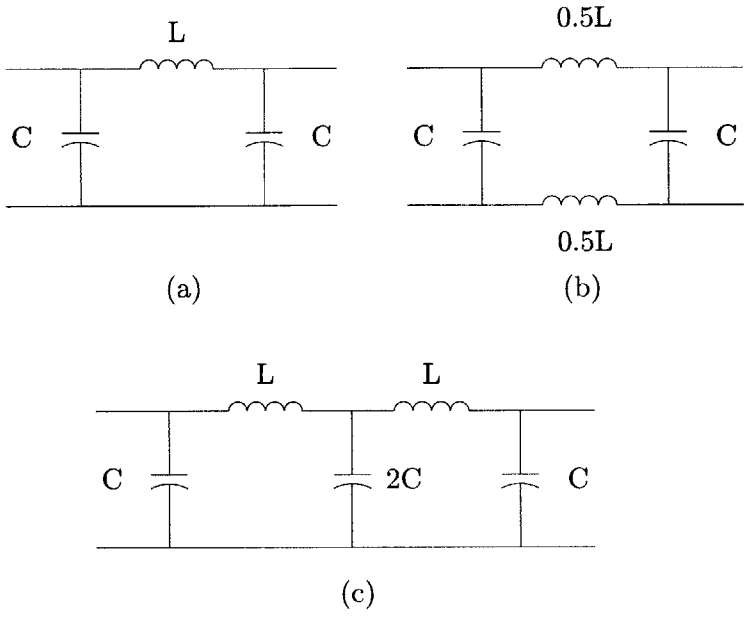

Figure 5-1: (a) One-stage π filter. (b) Balanced one-stage π filter. (c) Two-stage π filter.

The π filter is suitable for dc applications where the switching frequency is high enough so that the capacitor connected to the load can supply enough current to the PWM switches without being excessively large. In these applications, however, the source impedance should be taken into consideration, as explained in the last paragraph.

5.1.2 T Filter

The T filter is also a third order filter (Fig. 5-2,) which gives an 18 dB per octave roll-off slope. As for the π filter, the T filter can be cascaded to provide greater loss. The inductance can be split evenly between the high voltage line and the return path to create a balanced circuit. The T filter works well with low source impedance circuits, because it has an inductor on the source side.

The T filter should not be used in dc applications with switches. The inductor on the load side will cause serious problems during switching transitions, because it will not supply sufficient current to the switch. Furthermore, fast current transitions will induce high voltage spikes across the inductor, and increase the radiated noise level.

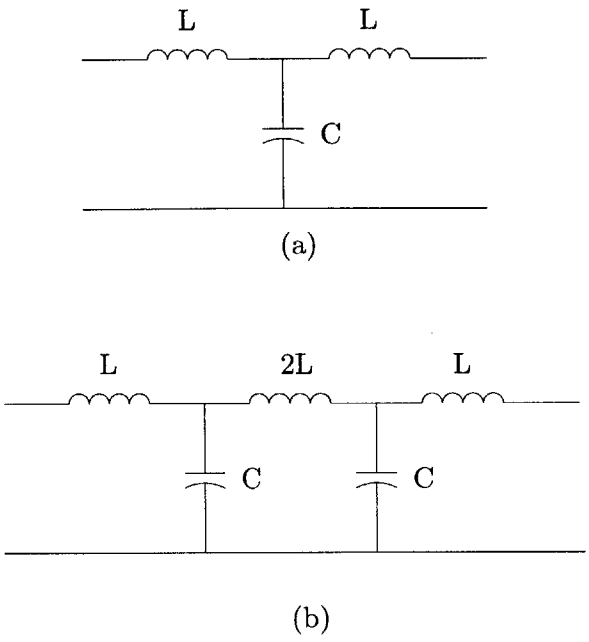

Figure 5-2: (a) One-stage T filter. (b) Two-stage T filter.

5.1.3 L Filter

Fig. 5-3 shows the L filter. The L filter combines advantages of both the π filter and the T filter. When the capacitor is connected on the load side, the L filter can deal with a low source impedance very well, and it has a low load side impedance. The L filter an ideal candidate for dc applications with switches, because when the capacitor is large enough, the filter can provide sufficient current to the switch during transitions. The only drawback of the L filter is that it is a second order filter; therefore it does not give as much roll-off slope as the other two types of filters do, i.e., to achieve the same amount of insertion loss at a certain frequency with the same number of stages, the L filter will have a lower cutoff frequency, which results in bigger components.

As for the π and the T filters, a higher order L filter can be constructed by cascading several one-stage L filters together. Moreover, a two-stage π filter will degrade to a two-stage L filter when the output capacitance of the source is on the same order of magnitude as, or less than the π filter capacitor.

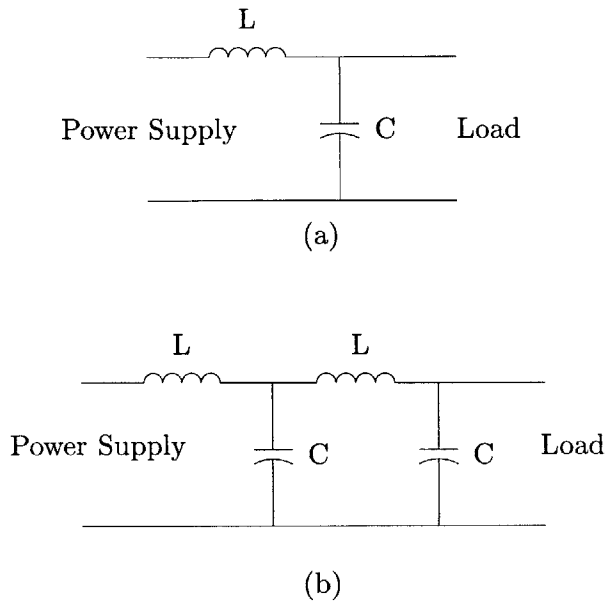

Figure 5-3: (a) One-stage L filter. (b) Two-stage L filter.

5.2 EMI Filter Requirements

With a list of advantages and disadvantages of different topologies available, it does not take very much effort to determine which topology should be applied to the PWM dc motor drive application. Since the load of the filter is a dc switching circuit, either the L filter or the π filter should be applied.

Even though the π filter provides a steeper roll-off slope than the L filter does, its operation can be greatly influenced by the output impedance of the source (or the load-side impedance of the LISN, if the goal of the filter design is to meet SAE J1113/41.) The L filter, on the other hand, has a much higher input impedance, and therefore, it is much more robust against the varying source impedance than the π filter is. In addition, the L filter requires fewer elements than the π filter, and it is easier to design. Therefore, the L filter topology (a balanced version of Fig. 5-3(a)) is chosen for this particular application.

5.3 Capacitor Value for the L Filter

Since the methodology of choosing filter elements is so flexible, it is much easier for the designer if some constraints can be applied to the design. constraints on the value of the capacitor for this particular application are given in this section, and the inductance required

to provide adequate insertion loss will be calculated in Section 5.4, after the damping circuit is considered.

The PWM circuit and its inductive load can be modeled as a current source with a trapezoidal waveform (Fig. 5-4). Assuming that the inductor in the L filter is large enough

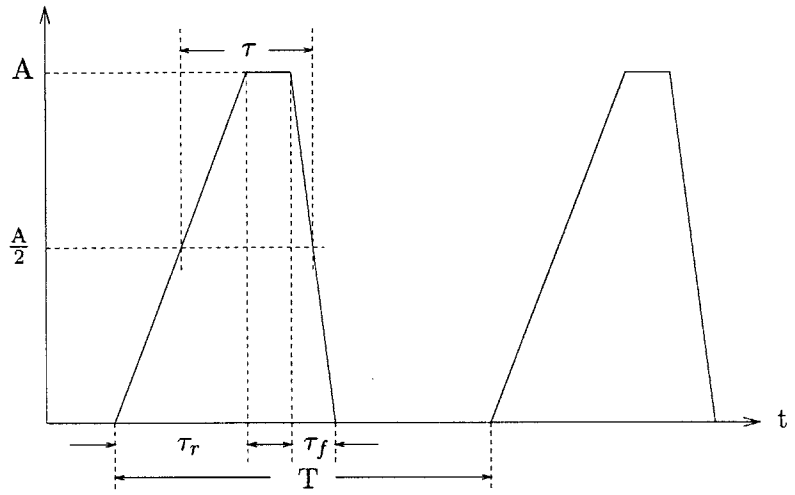

Figure 5-4: Line current waveform for a typical PWM drive with a resistive load.

such that the current flowing through it is a constant equal to I_{ave}, the current flowing through the current source is the sum of I_{ave} and the current going through the capacitor. Therefore, the charge needed to be stored in or extracted from the capacitor during different phases of the current source can be calculated as

$$\Delta Q = (I_{peak} - I_{ave})\, d\, T, \tag{5.1}$$

where I_{peak} is the amplitude of the current source waveform, I_{ave} is the inductor current, d is the duty ratio, and T is the switching period. The relationship

$$\Delta v = \frac{\Delta Q}{C} \tag{5.2}$$

implies that the capacitor has to be large enough so that the voltage ripple, Δv across the capacitor due to the stored charge variation, ΔQ does not affect the proper operation of the PWM circuit. I_{ave} can be expressed in terms of I_{peak} and d as

$$I_{ave} = I_{peak} d, \tag{5.3}$$

which gives

$$\Delta Q = I_{peak}\,(d - d^2)\,T. \tag{5.4}$$

where I_{peak} is a function of d and the load impedance. To simplify the calculation of ΔQ, I_{peak} is fixed to the maximum switch-on current flowing through the switch. Assuming that the maximum duty ratio for the PWM drive is 80%, this maximum switch-on current is measured to be 2.4 A. With I_{peak} fixed, Δ Q reaches its maximum value at a 50% duty ratio.

For the PWM drive to function properly, the voltage ripple across the capacitor should be less than 15% of the dc supply voltage. With 42 V supply and a 50μs switching period, the capacitance required for the L filter can be calculated as

$$\begin{aligned} C &= \frac{\Delta Q}{\Delta v} \\ &= \frac{I_{peak}\,(d - d^2)\,T}{\Delta v} \\ &= \frac{(2.4\,\mathrm{A})\,(.5 - .5^2)\,(50\mu\mathrm{s})}{(42\,\mathrm{V})(.15)} \\ &= 4.76\mu\mathrm{F}. \end{aligned} \tag{5.5}$$

The capacitor value is rounded up to 5μF.

5.4 Damping and Inductor Value for the L Filter

The Q value is a very important measure for the stability of the filter and the overall system [7]. A filter with a high Q value can cause ringing in the circuit. The voltage ripple due to the ringing can be large enough to affect the proper operation of the circuit or even damage the circuit.

The Q value of the filter can be reduced by adding damping to the filter. Two of the most common damping circuits are shown in Fig. 5-5. The configuration in Fig. 5-5 (a) is chosen for the PWM circuit, although the other configuration will work just as well. There are two LC loops in this configuration, LC_1, and LC_2. In general, the capacitor C_2 is much greater than C_1, which gives LC_2 a much lower cutoff frequency than LC_1. At the cutoff frequency of LC_1, LC_2 provides additional attenuation, and therefore, reduces the Q value of LC_1.

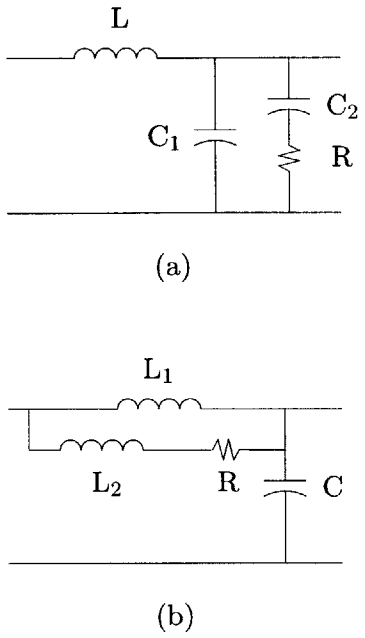

Figure 5-5: Two types of damping circuit.

In Fig. 5-5(a), C_1 is the capacitor in the original L filter whose value is calculated in the previous section. The capacitance of C_2 should be at least five times larger than C_1. A 100 μF electrolytic capacitor is used for C_2. R should be small to minimize the output impedance of the filter. It is set to be 0.5 Ω. The output impedance can be expressed as

$$\begin{aligned} Z_{out} &= \frac{L\,s\,(1+R\,C_2\,s)}{1+R\,C_2\,s+L\,(C_1+C_2)\,s^2+L\,R\,C_1\,C_2\,s^3} \\ &\approx \frac{L\,s}{1+\frac{L}{R}\,s+L\,C_1\,s^2}. \end{aligned} \tag{5.6}$$

The gain of this filter can be expressed as

$$\begin{aligned} GAIN &= \frac{1+R\,C_2\,s}{1+R\,C_2\,s+L\,(C_1+C_2)\,s^2+L\,R\,C_1\,C_2\,s^3} \\ &\approx \frac{1}{1+\frac{L}{R}\,s+L\,C_1\,s^2}, \end{aligned} \tag{5.7}$$

which can be used to calculate the inductance [7].

The measurement result in Chapter 4 shows that the greatest attenuation needed to meet Class 5 on Standard SAE J1113/41 is 36 dB, which occurs at 150 kHz. A 6 dB margin is usually recommended in EMI filter design, which increases the total attenuation at 150 kHz to 42 dB. The inductor value is calculated using Eq. 5.7 and is equal to 27.4μH. The balanced

configuration of the L filter will be used, and each of the inductors will be 15μH.

5.5 Filter Component Selection and Layout

All capacitors and inductors have parasitic resistance, capacitance and inductance associated with them, and these parasitic components can greatly affect the performance of these components over the frequency range specified by the EMI standard. For instance, the leads of a capacitor have some finite inductance. At very high frequencies, these leads behave as high impedances. When these parasitic components cannot be neglected, the filter no longer behaves the way it is designed, and fails to provide the insertion loss needed for reducing the noise to an acceptable level.

The equivalent circuits for capacitors and inductors are shown in Fig. 5-6. The equivalent

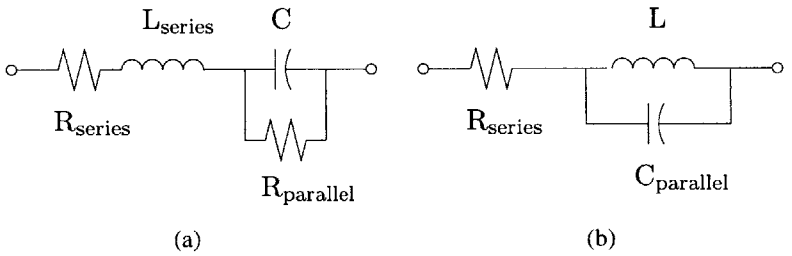

Figure 5-6: Equivalent circuits for (a) capacitors, and (b) inductors.

impedance of these two types of components can be expressed as

$$\begin{aligned} Z_C &= R_{series} + j\,\omega\,L_{series} + \frac{R_{parallel}}{1 + j\,\omega\,R_{parallel}\,C} \\ &\approx R_{series} + j\,\omega\,L_{series} + \frac{1}{j\,\omega\,C}, \end{aligned} \tag{5.8}$$

and

$$\begin{aligned} Z_L &= R_{series} + \frac{j\,\omega\,L}{1 - \omega^2\,L\,C_{parallel}} \\ &\approx \frac{j\,\omega\,L}{1 - \omega^2\,L\,C_{parallel}}. \end{aligned} \tag{5.9}$$

The impedance of a component can be easily measured with an impedance analyzer. An-

other way to evaluate the performance of capacitors and inductors is to look at the insertion loss they provide.

The performance of the inductors and capacitors depends on their physical structure and the material used to construct them. Figure 5-7 shows usable frequency ranges for various types of capacitors. The solid lines indicate usable frequency ranges for the regular capacitors, and the dashed lines show those for the high quality capacitors of the same type. Unlike capacitors, there are many parameters that characterize the behavior of inductors.

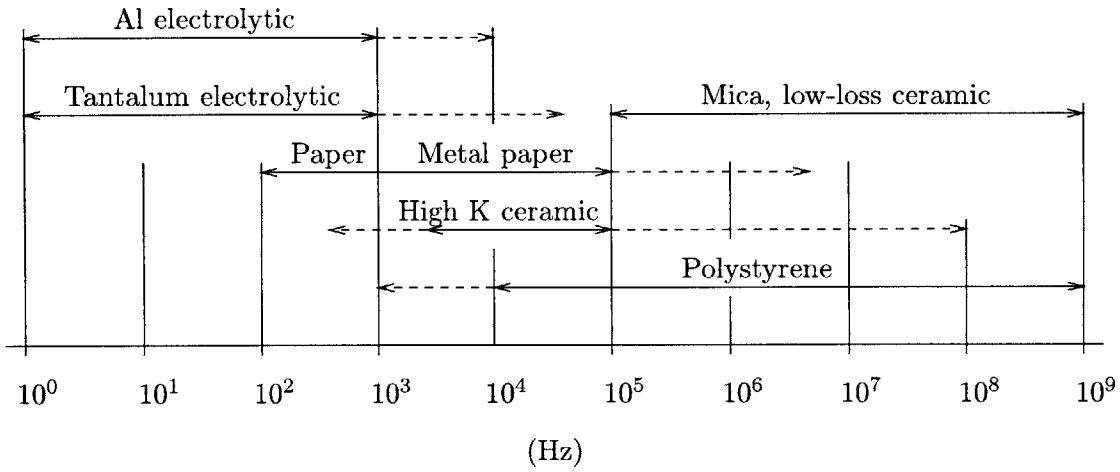

Figure 5-7: Usable frequency ranges for various types of capacitors.

Consequently, different manufacturers tend to make inductor cores with various types of material and different physical shapes. It is hard to categorize them in general [8]. Iron powder cores are a good candidate to construct inductors for their wide operating frequency ranges.

An electrolytic capacitor is the best choice for the 100 μF capacitor, and a film capacitor can be used for the 5 μF capacitor. To compensate the poor high frequency performance of the electrolytic and film capacitors, a small ceramic disk capacitor of .1 μF will be added and described in Chapter 6. Two T68-26A iron powder cores from Micrometals are used to construct the inductors [9].

Besides the physical structure of the components, their placement on the printed circuit board (PCB) also has a great impact on the performance of the components. The capacitor should be placed as close as possible to the switch, and its leads should be as short as possible to reduce its parasitic inductance. The inductor turns should be evenly separated,

and as widely as possible to reduce the parasitic capacitance. The measured insertion loss of the designed filter is shown in Fig. 5-8.

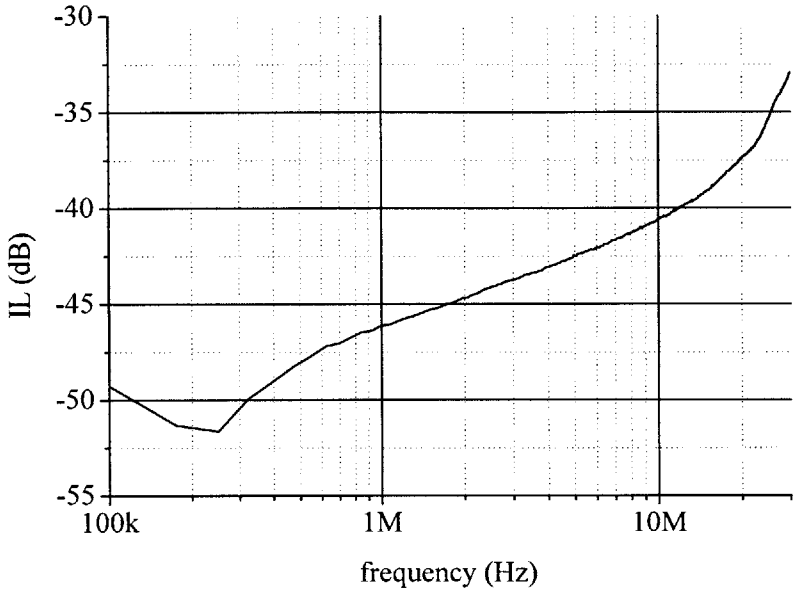

Figure 5-8: Insertion loss of the EMI filter.

Chapter 6

EMI Measurement with EMI Filter

This chapter presents EMI measurement results with the EMI filter designed in Chapter 5 inserted in the PWM drive circuit. As in Chapter 4, both the frequency and time domain measurements are recorded, and a detailed analysis is provided.

System designers often overlook EMC issues until the last stage of the design process. The EMI level could be unnecessarily high due to improper routing or placement of components. Proper circuit layout and grounding can make EMI filter design much easier and cheaper. In this chapter, the measurement result will also show how important a careful layout is for the performance of the system. Necessary adjustments for both the filter and the original PWM drive circuit are also discussed in detail.

6.1 EMI Measurement before Modification

The filter is inserted between the LISN and the PWM drive. Figure 3-1, repeated here as Fig. 6-1, shows the positions of the LISN and the PWM dirve. Figure 6-2 shows the EMI measurement for the PWM drive circuit with the filter inserted. Even though the EMI level meets the design objective quite nicely at 150 kHz, it peaks at 8.8 MHz and gives an EMI level 30.6 dB higher than the limit. This peak is due to the parasitic components of the film capacitor, the excessive wiring within the PWM drive circuit, and the semiconductor switches. These parasitic inductances and capacitances form an LC loop with a cutoff frequency at the peak frequency.

The parasitic inductance of the wiring and the motor, along with the parasitic capacitor of the Schottky diode (shown in Fig. 6-3) creates another LC loop with a much higher cutoff

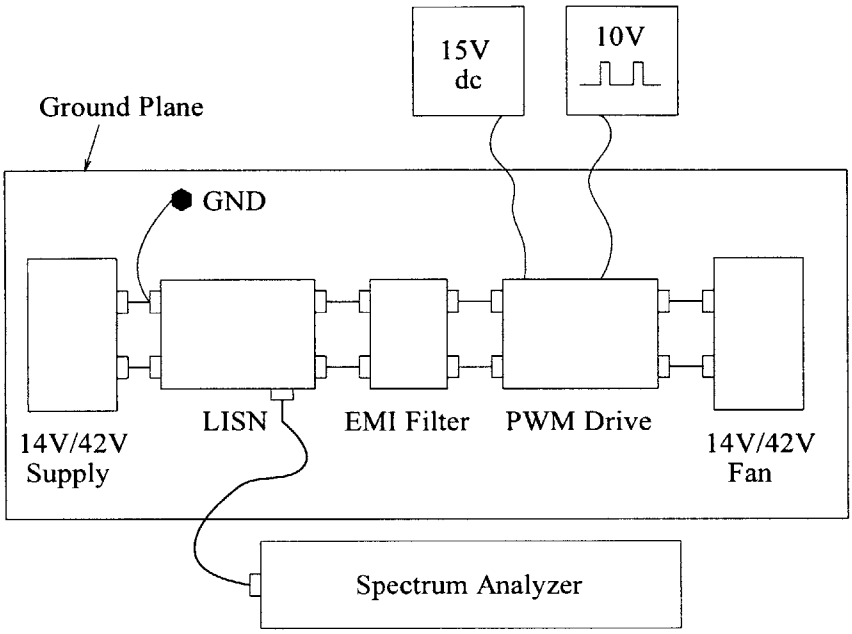

Figure 6-1: Test bench layout with the EMI filter.

frequency, typically around 66 MHz. This high frequency noise is radiated by the wiring and coupled back to the LISN.

6.2 EMI Measurement after Modification

To suppress the noise peak at 8.8 MHz, the high frequency performance of the filter should be improved and the excessive wiring on the PCB board should be eliminated.

To achieve a better high frequency response, a .1 μF ceramic capacitor is connected in parallel with the large 5 μF film capacitor. This capacitor should be physically placed as close to the drain of the MOSFET switch as possible, and the leads of the capacitor should be minimized to reduce the parasitic inductance due to wiring. To reduce the noise peak in the frequency range from 30 MHz to 108 MHz, another .1μF capacitor is connected between the source of the MOSFET and ground, and it, again, should be placed as close to the MOSFET as possible. In addition, the PWM drive circuit is reconstructed with a better layout to eliminate excessive wiring.

Figure 6-4 shows the EMI measurement after the above modifications have been made. The result shows that the amplitude at 8.8 MHz is reduced by 20 dB, and the peak shifts to a lower frequency of 5.1 MHz. The new peak is, however, still 7.48 dB higher than the

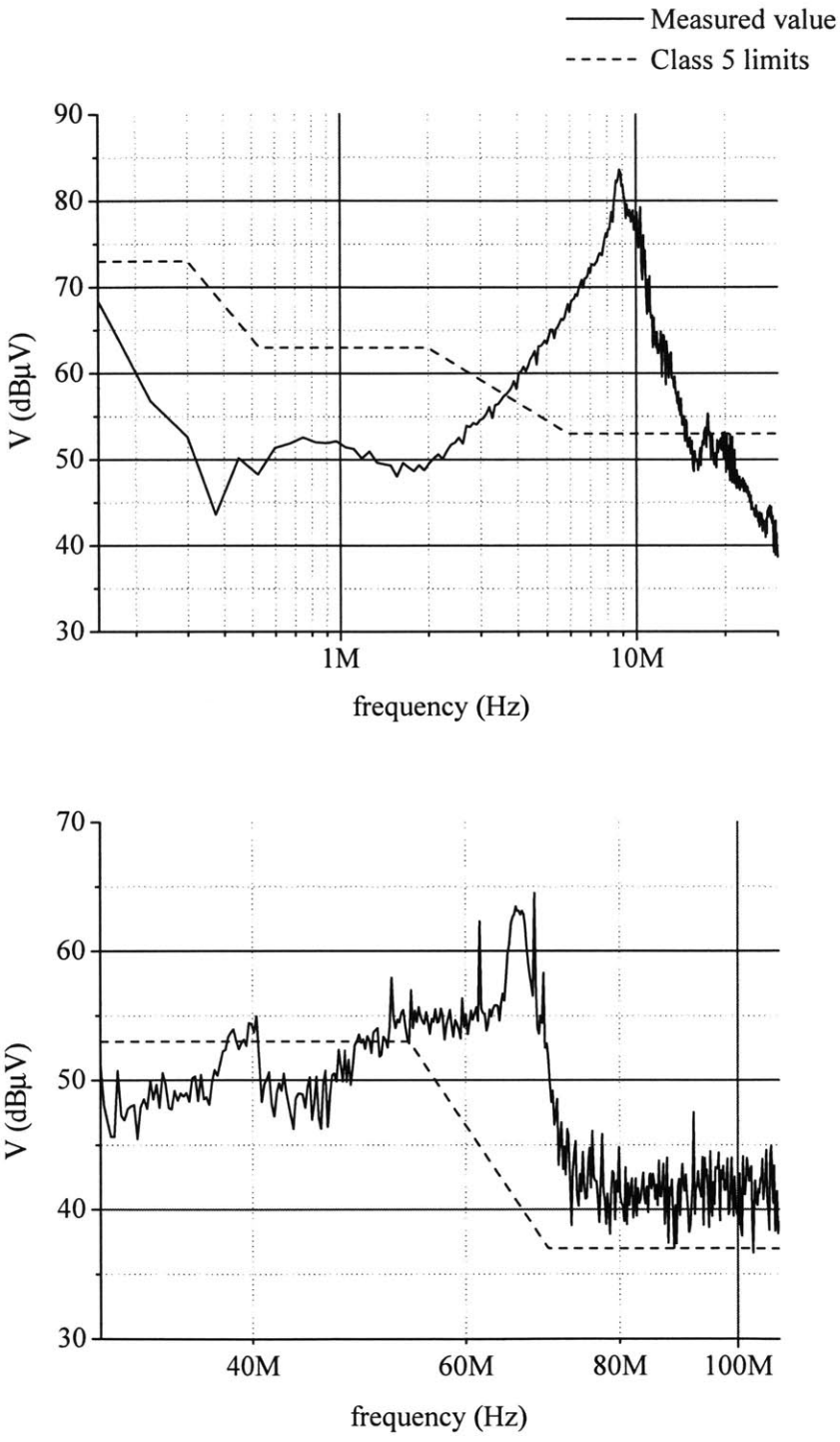

Figure 6-2: EMI level before modification.

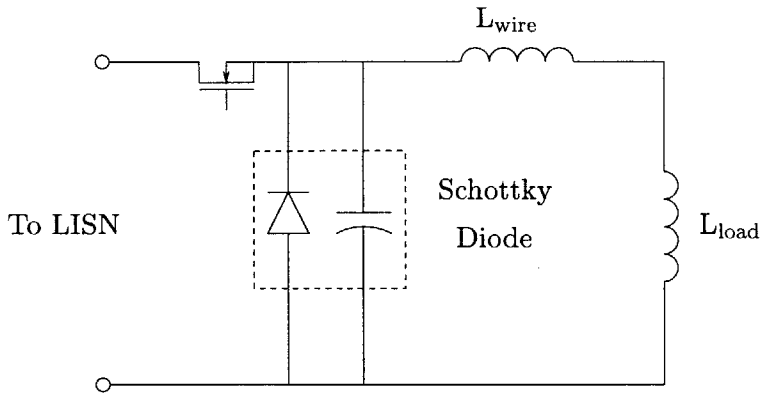

Figure 6-3: LC loop formed by the parasitic components of the Schottky diode and the wiring.

limit.

Even though the noise peak at 66 MHz is reduced by 10 dB, it does not meet the limit for Class 5. In this frequency range, the filter inductor becomes capacitive for most types of core materials and the filter capacitor inductive. The noise in this frequency range propagates from the wiring between the PWM drive and the motot to the LISN through electromagnetic coupling. Tighter packaging and good shielding will bring the noise level in this frequency range below the limit.

6.3 Further Improvement

There are several things that can be done to make the filter design easier besides making the circuit more compact, and to have shielding around it. Different types of diodes can be considered to replace the Schottky diode used in the drive, small gate resistance can be used to change the di/dt level of the current. A small capacitor can be added between the drain and the gate of the MOSFET awitch to reduce the Miller effect. The voltage waveform across the drain and the source of the MOSFET switch will be improved by reducing the Miller effect.

The same PWM drive circuit is used for both the 14 V and the 42 V load to do a reasonable comparison. There is no reason, however, not to use a diode rated for 42 V, but smaller current for the 42 V load. For a diode, smaller current rating means smaller cross section area, or smaller parasitic capacitance. Smaller parasitic capacitance of the

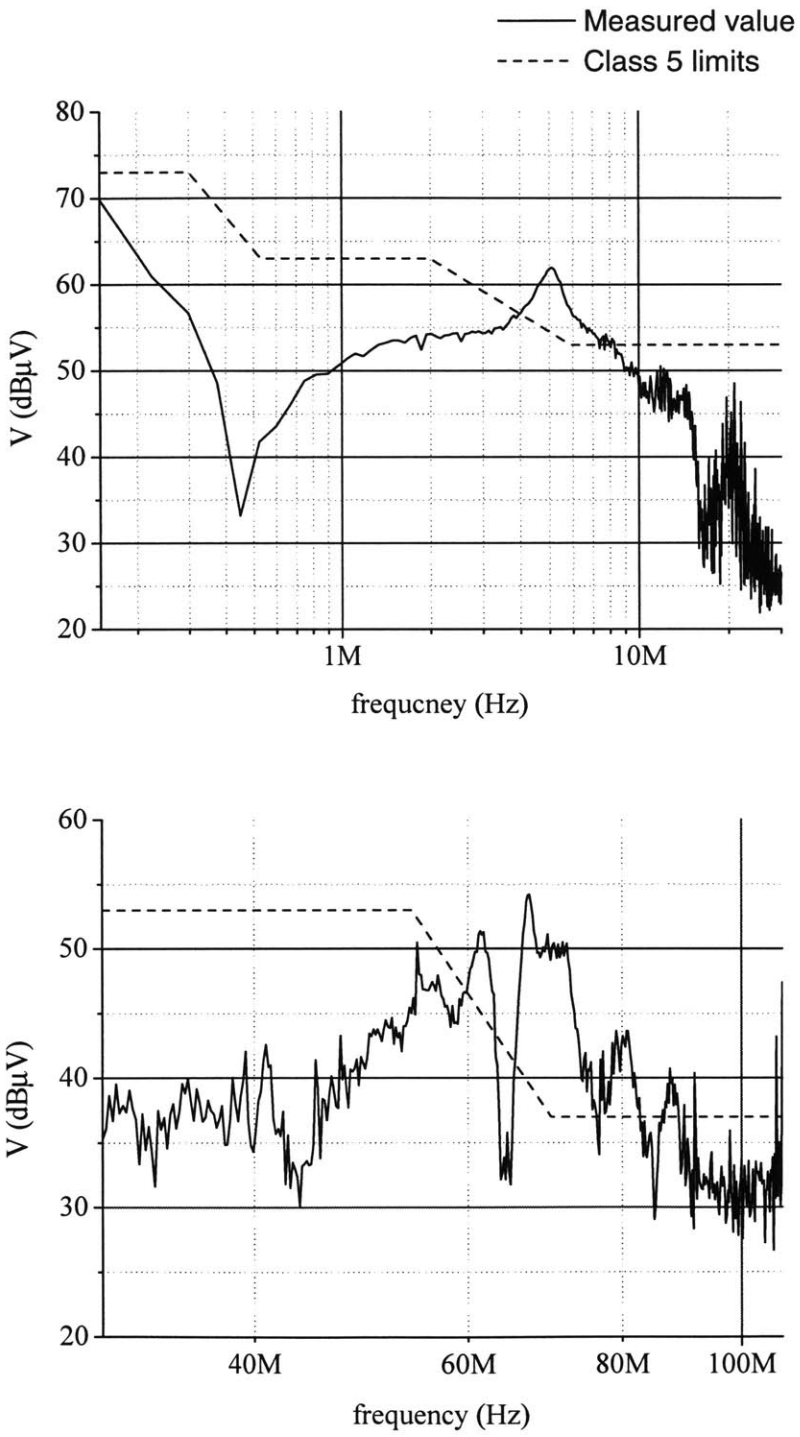

Figure 6-4: EMI level after modification.

diode can help reduce the current spikes during turn on, which, in turn, will bring the noise level down. Furthermore, a soft recovery diode can be used in this particular application, because power consumption of the switch is not an issue here, as long as it does not affect the normal operation of the switch.

The effect of the gate resistance on EMI level in the high frequency range was explained in Chapter 4. As long as the gate resistance is not so large that it forces the MOSFET transistor to its active region, it should be applied.

The Miller effect has some nonlinear effects on the voltage across the MOSFET switch, which will introduce noise into the system. A capacitor on the order of a few nF can be added between the drain and the gate of the MOSFET transistor to reduce the Miller effect.

Chapter 7

Conclusion

This chapter concludes this research project, and provides recommendations for future development of the PWM dc motor drive system in automotive applications from an EMI perspective.

This research project investigated EMI behavior of PWM dc motor drives in a typical automotive application — blower-fan motor control. The investigation can be divided into five phases: theoretical development, experimental test setup, EMI measurement without filter, EMI filter design, and EMI measurement with EMI filter, and these five phases were described in chapters 2 to 6.

Chapter 2 started with modelling the line current in a typical PWM dc motor drive application as a trapezoidal waveform. A mathematical model of the spectrum for this line current was then established through Fourier analysis. This model, along with a simple LISN model, was used to calculate the EMI level for the PWM drive. One example was given in Chapter 4.

In Chapter 3, a prototype PWM motor drive was designed and constructed. A test setup for EMI measurements was built according to the specifications listed in SAE J1113/41. A supporting device for accurate measurements, the rectangular wave generator, was also built and added on to the PWM drive circuit.

Chapter 4 involved collecting and analyzing EMI measurement results for the PWM motor drive under different load conditions and duty ratios. The effect of gate resistance on the EMI level was also explored.

Chapter 5 focused on different aspects of EMI filter design. Such issues as topologies,

Q value and damping, parasitic components and frequency response of capacitors and inductors were considered. An EMI filter for the prototype PWM drive was designed and constructed.

In Chapter 6, the performance of the EMI filter built in the previous phase was evaluated. Adjustments were made for the original PWM drive circuit to improve the high frequency performance of the entire system.

The theoretical model developed in the second phase was found to be very accurate in determining the EMI level of the PWM drive. The calculated result accurately matched the measurement result.

Measurement results in the third phase show that the conducted emission of a PWM dc motor drive depends on four parameters of the line current waveform — the relative rise time, the relative fall time, the duty ratio and the amplitude. The first three parameters had a great impact at frequencies higher than 1 MHz, while the last parameter determined the EMI level over the entire frequency range. Since the amplitude is a function of duty ratio for a particular load, the greater the duty ratio, the higher the EMI level.

For two different loads with similar power rating, the one with higher voltage rating had lower current amplitudes for corresponding duty ratio. This indicated that the load with the higher voltage rating has a lower EMI level than the other at low frequencies, i.e., 150 kHz, which is the frequency requiring the greatest attenuation, or matters the most. At higher frequencies, the other three parameters start to take effect, and the overall effect can only be determined after a detailed calculation using the theoretical result developed in the second phase.

The high frequency performance of the filter was limited by the packaging technology and components available for this project, which can be easily overcome during system integration. The behavior of the EMI filter can be correctly predicted if the parasitic capacitance and inductance for the switches and wiring are available.

Appendix A

Insertion Loss Calculation

The performance of an EMI filter is evaluated by insertion loss, instead of attenuation. Insertion loss of a device under test (DUT) is defined as

$$\begin{aligned} IL &= 10 \log(\frac{P_b}{P_a}) \\ &= 20 \log(\frac{V_b}{V_a}), \end{aligned} \tag{A.1}$$

where P_b and P_a are the power delivered to the load of a reference circuit before and after the DUT is inserted into the reference circuit, and V_b and V_a are the corresponding voltages. Fig. 2-5 is duplicated here to show a typical way of measuring insertion loss.

A DUT can be represented by a matrix under two-port network theory, and the insertion loss of the DUT can be calculated with this matrix. The most common matrix forms used to calculate insertion loss are the A and the Z matrix. The A matrix is also known as the chain matrix. It has the advantage of expressing a complicated circuit as a product of many matrices, each of which characterizes a cascaded part of the overall circuit.

The A matrix relates the input and output voltages and current in the following way:

$$\begin{pmatrix} V_1 \\ I_1 \end{pmatrix} = \begin{pmatrix} A_{11} & A_{12} \\ A_{21} & A_{22} \end{pmatrix} \begin{pmatrix} V_2 \\ -I_2 \end{pmatrix}. \tag{A.2}$$

V_1, I_1, V_2 and I_2 are defined in Fig. A-2. The Z matrix is defined as

$$\begin{pmatrix} V_1 \\ V_2 \end{pmatrix} = \begin{pmatrix} Z_{11} & Z_{12} \\ Z_{21} & Z_{22} \end{pmatrix} \begin{pmatrix} I_1 \\ I_2 \end{pmatrix}. \tag{A.3}$$

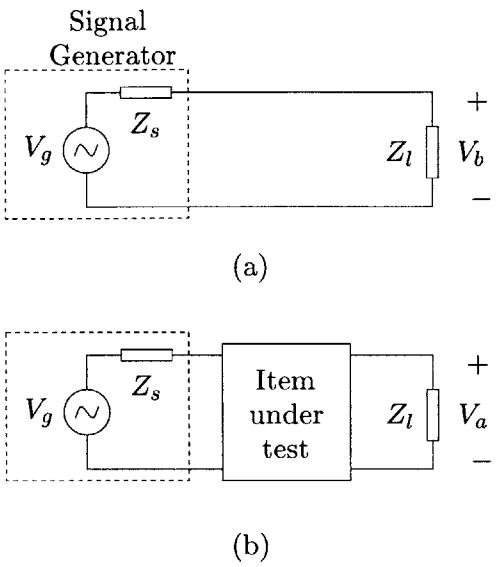

Figure A-1: Insertion loss definition. (a) Reference circuit. (b) Test item inserted.

The relationship between the A parameters and the Z parameters are

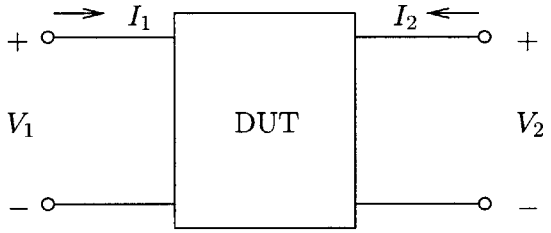

Figure A-2: Voltages and currents definition for a two-port network.

$$\begin{aligned} A_{11} &= \frac{Z_{11}}{Z_{21}} \\ A_{12} &= \frac{Z_{11}Z_{22}}{Z_{21}} - Z_{12} = A_{11}Z_{22} - Z_{12} \\ A_{21} &= \frac{1}{Z_{21}} \\ A_{22} &= \frac{Z_{22}}{Z_{21}}. \end{aligned} \tag{A.4}$$

Eq. A.2 implies that

$$V_2 = Z_{21}I_1 + Z_{22}I_2$$

$$= Z_{21}I_1 - Z_{22}\frac{V_a}{Z_l}, \tag{A.5}$$

or

$$I_1 = \frac{V_a}{Z_{21}}\left(1 + \frac{Z_{22}}{Z_l}\right) \tag{A.6}$$

Since

$$\begin{aligned} V_1 &= V_g - I_1 Z_g \\ &= Z_{11}I_1 + Z_{12}I_2, \end{aligned} \tag{A.7}$$

V_g can be expressed as

$$\begin{aligned} V_g &= (Z_{11} + Z_g)I_1 - Z_{12}\frac{V_2}{Z_l} \\ &= \left(\frac{(Z_{11} + Z_g)(Z_{22} + Z_l)}{Z_{21}Z_l} - \frac{Z_{12}}{Z_l}\right) V_a. \end{aligned} \tag{A.8}$$

V_b can be expressed in terms of V_g as

$$V_b = \frac{Z_l}{Z_l + Z_g}V_g, \tag{A.9}$$

and the insertion loss is

$$\begin{aligned} IL &= 20\ \log\left(\frac{V_b}{V_a}\right) \\ &= 20\log\left|\frac{(Z_{11} + Z_g)(Z_{22} + Z_l) - Z_{12}Z_{21}}{(Z_g + Z_l)Z_{21}}\right| \end{aligned} \tag{A.10}$$

Applying the relationship between the A parameters and Z parameters, the insertion loss can be expressed as

$$IL = 20\log\left|\frac{A_{11}Z_l + A_{12} + A_{21}Z_gZ_l + A_{22}Z_g}{Z_g + Z_l}\right|. \tag{A.11}$$

This result is used to calculate the insertion loss of the LISN in Chapter 3.

Appendix B

Matlab Code

The matlab codes listed in this Appendix are used to calculate the spectrums of the trapezoidal current waveform of the PWM drive and the noise, and the insertion loss of the LISN.

The first and second functions are used to calculate the spectrums for the current waveform and the noise.

```
function trapfreq(A, R, F, d, fsw)
% File trapfreq.m
% This function calculates the spectrum of a periodic
% trapezoidal waveform.

% A: amplitude
% fsw: switching frequency
% R: rise time/period
% F: fall time/period
% d: duty ratio
% step, step1, step2: increments for different resolution
% k: harmonic number
% S: 20*log|S(k)|
% kcx: cutoff harmonic numbers;
% S1: the first segment of the envelop;
% n1: index for S1;
```

```
% S2: the second segment;
% n2: index for S2;
% S3: the third segment;
% n3: index for S3.
% S4: the forth segment;
% n4: index for S4.

step=1;
step1=.2;
step2=.6;
initk=1;
finalk=3000;
% Calculate the rms value
A=A/sqrt(2);
k=initk:step:finalk;
fS=fsw*k;
ymin=10;
ymax=110;

% Calculate the spectrum
pid=pi*d;
% sinc(x)=sin(pi*x)/(pi*x)
S=20*log10(A/pi)+120+20*log10(abs(exp(j*pid*k)...
   .*sinc(R*k)-exp(-j*pid*k).*sinc(F*k))./k);

% Calculate the envelop.
S1a=20*log10(A/pi)+120+20*log10(abs(exp(j*pid)...
   *sinc(R)-exp(-j*pid)*sinc(F)));

kc1=2/sqrt((sinc(R)+sinc(F))^2*sin(pid)^2+(sinc(R)...
   -sinc(F))^2*cos(pid)^2);
n1=1:step1:kc1;
```

```
S1=ones(1,size(n1,2));
S1=S1*S1a;

if R>F
alpha=R;
beta=F;
else
alpha=F;
beta=R;
end

kc2=1/(pi*alpha);

n2=kc1:step2:kc2;
S2a=20*log10(A/pi)+120;
S2=S2a+20*log10(2./n2);

kc3=1/(pi*beta);
n3=kc2:step2:kc3;
S3a=20*log10(A)+120;
S3=S3a+20*log10(1/pi*(1.+kc2./n3)./n3);

n4=kc3:step:finalk;
S4a=20*log10(A)+120;
S4=S4a+20*log10((1/R+1/F)/pi^2./n4.^2);

kenv=[n1 n2 n3 n4];
fenv=fsw*kenv;
env=[S1 S2 S3 S4];

figure(1)
semilogx(fS,S,'b-',fenv,env,'r-'), grid on
```

```
xlabel('frequency (Hz)')
ylabel('S(f) dB')
axis([20e3 40e6 ymin ymax])

% Uncomment the following lines to calculate the noise
% spectrum

%[gainS, gainenv]=LisnIM1(fS,fenv);
%S=S+gainS;
%env=env+gainenv;
%figure(2)
%semilogx(fS,S,'b-',fenv,env,'r-'), grid on
%xlabel('f')
%ylabel('S(f) dBuV')
%axis([20e3 108e6 ymin ymax+10])

% EOF

function [gainS,gainenv]=LisnIM1(fS, fenv)
% File LisnIM1.m
% This function calculates the load side impedance
% of the LISN while the source side terminals are
% shorted.
L=5e-6;
C2=1e-7;
R2=50;

% gainS is used to calculate the EMI spectrum
wS=2*pi*fS;
Zl=j*wS*L;
Zc2=1./(j*wS*C2);
Zsr=Zc2+R2;
gainS=20*log10(abs(R2*Zl./(Zl+Zsr)));
```

```
% gainenv is used to calculate the envelop of the
% EMI spectrum
wenv=2*pi*fenv;
Zl=j*wenv*L;
Zc1=1./(j*wenv*C1);
Zc2=1./(j*wenv*C2);
Zsl=Zl+Zc1+R1;
Zsr=Zc2+R2;
gainenv=20*log10(abs(R2*Zl./(Zsr+Zl)));

%EOF
```

The third file is used to calculate the insertion loss of the LISN.

```
function IL=LisnIL
% File LisnIL.m
% This function calculates the insertion loss of the LISN.
% these parameters are defined in Fig. 3-4.
R1=5.9;
R2=1e4;
L=5e-6;
C1=1e-6;
C2=1e-7;

% The source and load impedances of the reference circuit.
Zg=50;
Zld=50;

% The insertion loss will be calculated from 100kHz to 30MHz.
f=1e5:1e4:3e8;
w=2*pi*f;
Zl=j*w*L;
```

```
Zc1=1./(j*w*C1);
Zc2=1./(j*w*C2);
Zs=R1+Zc1+Zl;

% Solve for A parameters.
A11=1+Zc2/R2;
A12=Zc2;
A22=Zc2./Zs+1;
A21=1./Zs+A22/R2;

% Use the result derived in Appendix A.
% The final result is negated to match the measurement.
IL=abs((Zld*A11+A12+A21*Zg*Zld+Zg*A22)/(Zg+Zld));
IL=-20*log10(IL);
figure(1)
semilogx(f,IL)

% EOF
```

Bibliography

[1] J.G. Kassakian, Hans-Christoph Wolf, J.M. Miller, and C.J. Hurton. Automotive electrical systems circa 2005. *IEEE Spectrum*, August 1996.

[2] László Tihanyi. *Electromagnetic Compatibility in Power Electronics.* IEEE Press, 1995.

[3] Mark J. Nave. *Power Line Filter Design for Switched-mode Power Supplies.* Van Nostrand Reinhold, 1991.

[4] A. Nagel and R.W. De Doncker. Some simple approximation of interference spectra. *EPE'97, 7th European Conf. on Power Electronics and Applications*, September 1997.

[5] David Morgan. *A Handbook for EMC Testing and Measurement.* Peter Peregrinus Ltd., 1994.

[6] SAE J1113/41. *SAE Surface Vehicle Electromagnetic Compatibility (EMC) Standards Manual.* Society of Automotive Engineers, Inc., Warrendale, PA, 1997 edition, July 1995.

[7] T.K. Phelps and W.S. Tate. Optimizing passive input filter design. In *Proc. of the 6th National Solid-State Power Conversion Conf.*, pages G1–1–G1–10. Academic Press, May 1979.

[8] M.F. Schlecht J.G. Kassakian and G.C. Verghese. *Principles of Power Electronics.* Addison-Wesley Publishing Company, 1991.

[9] Issue H. *Power Conversion & Line Filter Applications.* Micrometals, Inc., Anaheim, CA, 1995.